Title
Impaired sensory adaptation in the Fmr1-/- mouse model of autism

Author
He, Cynthia

Publication Date
2017

Peer reviewed|Thesis/dissertation

UNIVERSITY OF CALIFORNIA

Los Angeles

Impaired sensory adaptation in the *Fmr1*$^{-/-}$ mouse model of autism

A dissertation submitted in partial satisfaction of the

requirements for the degree Doctor of Philosophy

in Neuroscience

by

Cynthia He

2017

ABSTRACT OF THE DISSERTATION

Impaired sensory adaptation

in the *Fmr1*$^{-/-}$ mouse model of autism

by

Cynthia He

Doctor of Philosophy in Neuroscience

University of California, Los Angeles, 2017

Professor Carlos Portera-Cailliau, Chair

Sensory overreactivity is a common symptom in autism spectrum disorders (ASDs), including Fragile X Syndrome (FXS), and frequently leads to tactile defensiveness. In mouse models of ASDs, there is mounting evidence of neuronal and circuit hyperexcitability in several brain regions, which could contribute to sensory hypersensitivity. However, it is not yet known whether or how sensory stimulation might trigger abnormal sensory processing at the circuit level or abnormal behavioral responses in ASD mouse models, especially during an early developmental time when experience-dependent plasticity shapes such circuits. Using a new behavioral assay, we discovered exaggerated motor responses to whisker stimulation in young *Fmr1*$^{-/-}$ mice (postnatal days (P) 14-16), a model of FXS. Adult *Fmr1*$^{-/-}$ mice actively avoided the same stimulus, a sign of tactile defensiveness. Using a novel protocol for expressing and imaging GCaMP6s in L2/3 barrel cortex neurons of early postnatal mice, we found no differences between wild-type and *Fmr1*$^{-/-}$ mice in overall whisker-evoked activity, though 45% fewer neurons in

young *Fmr1*$^{-/-}$ mice responded in a time-locked manner. Notably, we identified a pronounced deficit in neuronal adaptation to repetitive whisker stimulation in both young and adult *Fmr1*$^{-/-}$ mice. Thus, impaired adaptation in cortical sensory circuits is a potential cause of tactile defensiveness in autism.

The dissertation of Cynthia He is approved.

Daniel H. Geschwind

Kelsey C. Martin

Sotirios Masmanidis

Marc Adam Suchard

Carlos Portera-Cailliau, Committee Chair

University of California, Los Angeles

2017

Table of Contents

List of Figures

List of Tables

Acknowledgments

In my experience, it takes a village to raise a graduate student, which makes this section of the dissertation perhaps the most important of all. I ask for the reader's indulgence as I thank my village.

First, I thank my advisor Dr. Carlos Portera-Cailliau. He was the very first faculty member with whom I interviewed at UCLA in December 2010, and from that first meeting, and every meeting since, he expressed great confidence in my abilities and potential as a scientist. He is deeply committed to his trainees and has demonstrated continual energy and enthusiasm for this project, as well as for my physician-scientist training. When I began graduate school I set several goals for myself, including: 1) learning a large volume of interesting science, 2) learning how to do *in vivo* neuroscience experiments, 3) figuring out something new and interesting about the Fragile X mouse model, and 4) writing a respectable paper of which I could be proud. Thanks to Carlos' mentorship, I have been able to accomplish all of these goals and more. On a lighter note, during my summer rotation in 2011, Carlos told me about how he had run with the bulls in Pamplona when he was younger, and he said that someday I would "do something crazy like that." I am still looking forward to finding out what that something will be.

I thank my friends and coworkers in the Portera-Cailliau lab for their support and good humor. Thanks to Drs. James Anstey, Tiago Gonçalves, Amaya Miquelajauregui, and Ricardo Mostany for teaching me the surgery and imaging techniques during my rotation. Thanks to Daniel Cantu for helping me get started after I officially joined the lab, and for our successful collaborations on surgeries, imaging, analysis, and baking. Thanks to Erica Arroyo for her solidarity in developmental experiments – we the few and proud! –, for her willingness to help troubleshoot endlessly, and for her excellent taste in the arts. Thanks to Dr. Anubhuti Goel for her mentorship and counsel, input in nearly all aspects of my project and paper, and generous teaching to me and to all other lab members. Thanks to Dr. Mate Marosi for his surgical and OIS expertise and teaching. Thanks to Dr. William Zeiger for our successful collaboration on the behavioral rig, and for his advice on both experiments and the physician-scientist trajectory. Thanks to Peter Pellionisz for his efforts on our microscope rigs. Thanks to Gengming Liu for his assistance in hardware assembly, and to him and Sheyda Mesgarzadeh for assistance on our behavioral rig and in my colony. Thanks to Grant Higerd and Sahana Kribakaran for their assistance with my colony. Thanks also to Dr. Daniel Fiole, Shilpa Mantri, Gunvant Chaudhari, Kaela Cohen, Steve Cohen, Chae Kwon, Michael Le, Aditi Newadkar, Satvir Saggi, and Barbara Todisco.

Substantial portions of the Introduction, Chapter 1, Chapter 3, and Discussion in this thesis originally comprised a manuscript submitted to the *Journal of Neuroscience*, entitled "Tactile defensiveness and impaired neuronal adaptation in the *Fmr1*$^{-/-}$ mouse model of autism." My

coauthors on this paper are Daniel Cantu, Shilpa Mantri, William Zeiger, Anubhuti Goel, and Carlos Portera-Cailliau (corresponding author). Carlos and I conceived the project and designed the experiments. Daniel and I developed the P1 injection and P14-16 imaging protocols, and wrote MATLAB code for data analysis. Will, Anu, and I developed the behavioral assay. I conducted the experiments and analyzed the data. Shilpa analyzed a subset of the behavioral data. Anu, Carlos and I interpreted the data. Carlos and I wrote the paper, with input from the other authors.

The overview of fluorescent calcium indicators in Chapter 2 of this thesis will form part of a review paper entitled "Fluorescent dyes for two-photon microscopy," on which I will be a coauthor. The first author is Daniel Fiole, a former postdoctoral fellow in the Portera-Cailliau lab.

The remainder of Chapter 2, detailing the P1 injection protocol, will comprise a methods/protocol paper entitled "Neonatal rAAV-GCaMP injection for imaging of cortical circuit activity in early postnatal mice," on which I will be the first author. The coauthors will be Daniel Cantu, Anubhuti Goel (who performed the whole cell recordings), and Carlos Portera-Cailliau.

My thesis work was supported by a Paul & Daisy Soros Fellowship for New Americans and a NIH NINDS National Research Service Award F30 Fellowship (NS093719), as well as the UCLA Medical Scientist Training Program (NIH NIGMS training grant GM08042). Coauthor Daniel Cantu was supported by a UCLA Neural Microcircuits training grant T32-NS058280 and a Eugene V. Cota-Robles Fellowship. This work was also supported by a Developmental Disabilities Translational Research Program grant #20160969 (The John Merck Fund), SFARI grant 295438 (Simons Foundation) and NIH NICHD grant R01 HD054453 to Carlos Portera-Cailliau.

I have benefited greatly from the warm neuroscience community at UCLA, which has supported me in my personal development as a trainee and has also enabled the success of this research endeavor. In particular, I thank my committee – Drs. Dan Geschwind, Kelsey Martin, Sotiris Masmanidis, and Marc Suchard – for their time and input throughout my training. I have benefited from Dan's expertise in autism at committee meetings, during this writing process, and also at a Cold Spring Harbor Laboratory seminar on Autism Spectrum Disorders. Kelsey was one of the MSTP directors when I applied and joined the program, and she has always made time for me and given me precisely the advice I needed. Sotiris is a remarkable teacher and has been a kind and wise sounding board during critical periods of my work. Marc has always pushed me to seek quantitative rigor and alternative approaches to thinking about my data.

My colleagues and I also thank Michael Einstein and Dr. Peyman Golshani for help with behavioral rig design; Drs. Patrick Mineault, Dario Ringach, Daniel Dombeck (Northwestern), Tsai-Wei Chen (Janelia), and Karel Svoboda (Janelia) for sharing MATLAB code for imaging analysis, as well as analysis ideas; Nicholas Hardy for input on behavioral data analysis; Dr. Mark

Reimers (Michigan State) for input on imaging analysis; Drs. Jason Moore and Dean Buonomano for input during the writing process; Kimberly Battista (Battista Illustration) for the P1 injection illustration; Dr. Andrew Keller for help with curve-fitting; and the Janelia GENIE project for the AAV GCaMP6s.

A special thanks to Dr. Nicholas Wisniewski, whose "Advanced Experimental Statistics" course established my approach to statistical analysis, and who was incredibly generous with his time and assistance well after the course had ended. Additional thanks to Christopher Griffis for his support as the TA for that course, and to Dr. Sitaram Vangala (CTSI Statistics Core) for his assistance as well.

I thank Lisa Barnhill and Sharon Li in the lab of Dr. Jeff Bronstein for amiably sharing their chemical hood and microscope with our lab. I thank other members of the UCLA Department of Neurology: Sarah Klein and Mark Almario in Fund Management, Brittany Howell and Samantha Dearn in the Education office, Margot Chang in Procurement, and Jaime Lopez in Custodial Services. I also thank Dr. Timothy Beyer for his kindness and wisdom.

I am grateful for the camaraderie of my classmates in the UCLA Interdepartmental Ph.D. Program for Neuroscience, as well as the support of Dr. Felix Schweizer, Jennifer Lee, my first rotation advisor Dr. Bennett Novitch, Dr. Albert Han, and Dr. Jack Feldman and the Neural Microcircuits Training Program. I also thank Dr. Anne Andrews for her support as faculty advisor for the Neuroscientific Methods course I co-taught with my classmate David DiTullio.

During graduate school I have been able to stay involved with the David Geffen School of Medicine, through the Medical Education Committee and Medical Student Council, and I thank Drs. Lee Miller, Neveen El-Farra, Thomas Drake, Mark Noah, and Deborah Lehman for their support in these activities. For the wonderful opportunities to lecture in the first-year curriculum, I thank Dr. Bruce Howard. I also thank Drs. Rachel Brook and Jennifer Yeung for the reimmersion preceptorship.

Having come to UCLA as a student in the Medical Scientist Training Program, I am very fond of my classmates in the entering class of 2011 and students across other years, and thank them for their friendship. I thank the current directors Drs. Carlos Portera-Cailliau and Leanne Jones, the past directors Drs. Kelsey Martin and Stephen Smale, and also Josephine Alviar, Judy Cervantes, Susie Esquivel, Phuong Macadangdang, and Dr. Sarika Thakur.

My previous teachers and mentors encouraged my interest in medicine and biomedical research, and enabled my present trajectory. I thank Ms. Courtenay Tessler and Mr. Scott Richardson at Davis Senior High School for their early belief in my potential. I thank Dr. M. Eric Gershwin at

UC Davis for being my first physician-scientist role model. I thank Dr. Ronald Wong and Dr. David Stevenson at Stanford for supporting my interest in neonatology and academic pediatrics and giving me a formative research experience. I thank Dr. Susan McConnell at Stanford, whose Developmental Neurobiology course ignited my interest in this research area.

My friends have buoyed me both before and throughout graduate school. I thank Elyse H., Laura B., Paras F., Justin L., Caroline L., Sophie R., Karthik S., Ivana J., Aaron L., Kevin L., Hua C., Janelle L., and David D. Thank you for all of our conversations (and commiserations), meals, adventures in LA and elsewhere, wine nights, and episodes of raucous laughter.

During graduate school my family expanded to include my wonderful in-laws: Lynne and Chuck, Grandma K, and Mike and Mel. Thank you for your support, encouragement, and the remarkable emotional boost that is my nephew.

My husband happens to be a brilliant and persevering scientist. He is also the funniest person I know, and has supported me with love and patience through every step of medical and graduate school, whether by listening to me recount all the minutiae of my day in lab, by proofreading my NRSA application on a Friday night, or by taking me out for therapeutic dinners. Thank you for our partnership, for being my home, and for your faith in me.

Finally, I want to acknowledge my parents and first teachers. My father is an immunologist and helped me do home science experiments from an early age, and he was also the first person to teach me about scientific rigor. My mother was the first woman in China to earn a Ph.D. in Computer Science Software, and became a tenured professor in the United States when I was still quite young. I did not understand, until I was much older, how amazing it was to grow up with such an inspiring example of a woman in STEM. To my parents: you are loving and kind, and you raised me to value educational opportunities, to believe in my abilities, and to give my best. For this and so much more, I cannot thank you enough.

Vita

EDUCATION

2011-- **David Geffen School of Medicine at the University of California, Los Angeles**
Medical Scientist Training Program, Interdepartmental Program in Neuroscience

2006-10 **Stanford University**

- B.S. in Biological Sciences – Neurobiology with Honors, with minor in Music

RESEARCH EXPERIENCE (since 2008)

2013-17 **Portera-Cailliau Lab** (Carlos Portera-Cailliau, M.D.-Ph.D., advisor)
Dept. of Neurology, UCLA David Geffen School of Medicine

- Thesis research: mechanisms of sensory hypersensitivity in the *Fmr1* knockout mouse model of Fragile X Syndrome.

2012 **Novitch Lab** (Bennett Novitch, Ph.D., advisor)
Dept. of Neurobiology, UCLA David Geffen School of Medicine

- Rotation project: investigation of embryonic motor column development, motor neuron and respiratory circuit function in a mouse model

2008-11 **Stevenson Lab** (David K. Stevenson, M.D., and Ronald J. Wong, M.D.-Ph.D., advisors)
Dept. of Pediatrics – Neonatology, Stanford School of Medicine

- Undergraduate and postbaccalaureate research: investigation of the effects of metalloporphyrins on the inhibition of heme oxygenase activity and subsequent effects on HO-1 gene expression in a mouse model of neonatal jaundice

PUBLICATIONS

He CX, Cantu DA, Mantri SA, Zeiger WA, Goel A, Portera-Cailliau C. *Tactile defensiveness and impaired neuronal adaptation in the Fmr1$^{-/-}$ mouse model of autism.* Manuscript submitted, 2017.

He CX, Portera-Cailliau C. *The trouble with spines in fragile X syndrome: density, maturity, and plasticity.* Neuroscience, 2013 Oct 22;251:120-8. PMCID: PMC3422423

He CX, Campbell CM, Zhao H, Kalish F, Schulz S, Vreman HJ, Wong RJ, Stevenson DK. *Effects of zinc deuteroporphyrin bis glycol on newborn mice after heme loading*. Pediatr Res. 70(5):467-72, 2011. PMCID: PMC3189293.

PRESENTATIONS:

Selected oral presentations:

He CX. *Impaired adaptation underlies tactile overreactivity in Fragile X mice.* Young Investigator Lecture Series, Integrative Center for Learning and Memory at UCLA, October 14, 2016.

He CX. *Linking defects in cortical network activity with altered sensory function in Fragile X mice*. Synapse To Circuit Club at UCLA, March 18, 2016.

He CX. *Linking defects in cortical network activity with altered sensory perception in Fragile X mice*. UCLA-Caltech Medical Scientist Training Program Tutorial Series, December 7, 2015.

He CX, Zhao H, Kalish F, Wong RJ, Stevenson DK. *Efficacy of zinc bis glycol porphyrin in inhibiting heme oxygenase activity in the heme-loaded newborn mouse*. Western Society for Pediatric Research, Carmel, CA, January 27-30, 2010.

Selected poster presentations:

He CX, Cantu DA, Portera-Cailliau C. *Linking defects in cortical network activity with altered sensory function in Fragile X mice.* Gordon Research Conference on Fragile X and Autism-Related Disorders, Mount Snow, VT, June 5-10, 2016.

He CX, Cantu DA, Portera-Cailliau C. *In vivo imaging of sensory-evoked cortical network activity in Fragile X mice.* Emerging Tools for Acquisition and Interpretation of Whole-Brain Functional Data, Janelia Research Campus, November 1-4, 2015.

DiTullio DJ*, He CX*, Andrews AM. *A student-led graduate seminar familiarizes students with neuroscientific techniques and improves oral presentation skills*. Society for Neuroscience Annual Meeting, Chicago, IL, October 17-21, 2015.

He CX, Cantu DA, Portera-Cailliau C. *Defects in whisker-evoked cortical network activity in Fragile X mice*. Neural Microcircuits Symposium, UCLA, May 14, 2015.

He CX, Morisawa T, Zhao H, Wong RJ, Stevenson DK. *The expression of heme oxygenase-1 following oral administration of chromium mesoporphyrin is age-dependent*. Pediatric Academic Societies Annual Meeting, Baltimore, MD, May 2 to 5, 2009. E-PAS2009:2842.404, 2009.

ACADEMIC AND RESEARCH AWARDS

2016 **First Place Poster** in Graduate Student category, Neurology Science Day, Department of Neurology, David Geffen School of Medicine at UCLA

2015 **National Research Service Award F30 Predoctoral Fellowship**, NIH National Institute for Neurological Disorders and Stroke

2013 **Paul and Daisy Soros Fellowship for New Americans**

2010 **Firestone Medal for Excellence in Undergraduate Research**, Stanford University
Clifford C. Lardinois, Sr. Oral Presentation Award, Western Student Medical Research Forum

2009 **Student Research Award**, Society for Pediatric Research
Major Grant, Stanford Undergraduate Advising and Research

2006 **U.S. Presidential Scholar**

- Recognized as the top female graduating senior in California. Attended National Recognition Week in Washington, D.C. as a guest of the U.S. Department of Education.

TEACHING EXPERIENCE

2014-17 **Invited lectures**: *Neonatal jaundice: physiological vs. pathological*, David Geffen School of Medicine at UCLA. January 16, 2014; January 15, 2015; January 14, 2016; January 12, 2017.

2015 **Student Instructor and Co-Coordinator** for Winter 2015 neuroscience seminar (*Neuroscientific Methods*), a student-led required course in the UCLA Interdepartmental Ph.D. Program in Neuroscience.

2007-09 **Residential Writing Tutor** in Stanford's Freshman-Sophomore College and Hume Writing Center

Introduction

One form, now another; one configuration, now another.
Like fossils locked deep in the folds of my brain,
outliving a time by telling its story. Like stars.

---from “The Enigma,” by Anne Stevenson

Autism and sensory overreactivity

Autism Spectrum Disorder (ASD) affects approximately 1 in 68 children in the United States (Christensen et al., 2016), with global prevalence estimated as 1% (Lai et al., 2014). This behavioral syndrome was originally described by Leo Kanner in 1943 (Kanner, 1943) and Hans Asperger in 1944 (Asperger, 1944). In their profiles of 11 and 4 children, respectively, both Kanner and Asperger described in exacting detail their subjects' difficulties with interpersonal communication and emotional expression, as well as an obsessive insistence on routines, all apparent at young ages and persisting over time. As Kanner wrote: "The outstanding, "pathognomonic," fundamental disorder is the children's *inability to relate themselves* in the ordinary way to people and situations from the beginning of life"; and, "The child's behavior is governed by an *anxiously obsessive desire for the maintenance of sameness* that nobody but the child himself may disrupt on rare occasions" (Kanner, 1943). Seventy years later, the American Psychiatric Association's Diagnostic and Statistical Manual (Fifth Edition) defined ASD using criteria that strikingly reflect Kanner and Asperger's original descriptions: 1) "persistent deficits in social communication and social interaction across multiple contexts," and 2) "restricted, repetitive patterns of behavior, interests, or activities," beginning during early development and causing functional impairment (American Psychiatric Assocation, 2013). Other frequent comorbidities include aggression, intellectual disability, attention deficit hyperactivity disorder, epilepsy, motor abnormalities, and gastrointestinal and sleep disturbances (Lai et al., 2014).

One DSM-defined sub-feature of restricted and repetitive behavioral patterns in ASD is sensory dysfunction hyperreactivity, hyporeactivity, or "unusual interest in sensory aspects of the environment" (American Psychiatric Assocation, 2013). Indeed, sensory dysfunction, especially

hypersensitivity causing overreactivity, occurs in 56-70% of individuals with ASD (Marco et al., 2011; Green et al., 2015). Sensory overreactivity commonly affects auditory, tactile, or visual processing, as well as multisensory integration, and may present as defensiveness, avoidance, or even sensory-seeking behavior (Marco et al., 2011; Green et al., 2015; Sinclair et al., 2016). One study of sensory and attentional dysfunction in 144 children with ASD found correlations between sensory overreactivity and social symptoms, as well as perseveration impairments (Liss et al., 2006). Indeed, sensory overreactivity that begins early in life likely contributes to other ASD symptoms, such as anxiety, hyperarousal and sleep disturbances, attention deficit, stereotyped behaviors or rituals, language delay, and learning difficulties (Ben-Sasson et al., 2007; Marco et al., 2011; Sinclair et al., 2016), and is thus a symptom of central significance in autism.

Over these seventy years, diagnostic sensitivity for autism has increased, with earlier clinical assessment and detection of atypical development enabling early interventions (Zwaigenbaum et al., 2015). However, treatments still rely primarily on behavioral therapies such as applied behavior analysis, structured teaching, and parent-mediated intervention, all of which aim to improve a child's cognitive, social, and emotional development and adaptive skills (Lai et al., 2014). Medications are used as adjunctive treatments for specific symptoms, such as antipsychotic drugs (risperidone) to reduce aggressive behaviors or stimulants (methylphenidate) to treat attention-deficit hyperactivity (Lai et al., 2014). None of these agents are disease-modifying, nor are they specific for autistic dysfunctions. The potential for adverse effects – both known and unknown – when these drugs are administered to young children provides significant cause for concern, as well as additional impetus to develop treatments targeted to ASD and its subsidiary functional deficits.

The origins of ASD are complex, involving a significant but multifactorial genetic component as well as epigenetic and environmental factors, which can converge, through neurobiological mechanisms still largely unclear, onto a wide range of clinical phenotypes (Lai et al., 2014; Parikshak et al., 2016). Because autism is a disorder of early neurodevelopment, with pathophysiological changes beginning in the gestational period (Ben-Ari, 2015), a truly disease-modifying treatment might have to be administered prenatally, or at least at a very young age. However, specific functional deficits such as repetitive behaviors, communication deficits, or sensory hyperreactivity are not consolidated until the postnatal period, under the influence of environmental cues and experience-dependent plasticity, and these deficits form a unique constellation in each affected child. It has been suggested that phenotypic heterogeneity in autism might not reflect only unique genetic or cellular pathologies, but rather a perturbation of network properties that emerge when neurons interact (Belmonte et al., 2004). As postulated by Liss and others, sensory overreactivity could be explained as a response to "overarousal" or "overexcitement" at the level of neural networks (Liss et al., 2006). Similarly, Markram & Markram have presented the "Intense World Theory" of ASD, wherein genetic predisposition, environmental influences, and/or toxic insult result in molecular pathologies that alter gene expression pathways. These molecular and cellular changes lead to hyperreactivity and hyperplasticity of neural microcircuits within multiple brain regions, hyperconnectivity between brain regions, and a variety of cognitive and functional changes including hypersensitivity, hyperattention, and hyperfear. According to this theory, the ultimate result of all of this "hyper-ing" is the child's perception of an overly intense and aversive world, to which the child responds with the clinically defined repetitiveness and social communication difficulty or withdrawal (Markram and Markram, 2010).

Because of ASD's molecular and phenotypic heterogeneity and the role of experience in shaping neurodevelopment, the development of effective treatments for specific functional deficits in ASD will likely require understanding the circuit-level alterations involved, including whether circuits are in fact "hyperreactive" or "overexcited." Electrophysiological studies (EEG) in children and adults with ASD have found some evidence, though inconsistent, for altered auditory brainstem responses, primary auditory cortex event-related potentials, gamma power, and gamma phase-locking (Marco et al., 2011; Sinclair et al., 2016). More strikingly, fMRI studies of children with ASD have showed increased resting-state functional connectivity and exposure-based activation in primary sensory cortical areas and the amygdala in response to visual, auditory, and tactile stimuli, with heightened activity correlating with parent-rated sensory overreactivity (Green et al., 2013, 2015, 2016). While these studies are crucial for evaluating network-level correlates of sensory dysfunction in humans, the EEG and fMRI methodologies lack single-neuron or microcircuit spatial resolution. To record network activity *in vivo*, with cellular resolution, the transgenic mouse models of the inherited or syndromic forms of ASD are particularly useful contexts within which to study circuit dysfunction related to autistic phenotypes (Gonçalves et al., 2013; Lu et al., 2016).

Fragile X Syndrome as a paradigm for studying autistic sensory overreactivity

In 1943, geneticists James Purdon Martin and Julia Bell described a sex-linked disorder of "mental deficiency" in eleven affected males within a single family, all born to apparently unaffected mothers (Martin and Bell, 1943). Based on their pedigree study, the authors hypothesized a sex-

linked recessive transmission. Over two decades later, Herbert Lubs used karyotyping in a study of four related males with mental retardation and described in their X chromosomes, as well as those of several unaffected relatives, a secondary constriction of the long arms (Lubs, 1969). His theory that the observed mental retardation was due to X-linked inheritance of this "marker X chromosome [….] a new type of cytogenetic abnormality in man" (Lubs, 1969) was borne out by subsequent work confirming the "fragile" chromosomal defect (Sutherland, 1977) and, crucially, demonstrating that the original probands described by Martin & Bell and other members of the same family in fact carried the fragile X chromosome (Richards et al., 1981). As a result the disorder of "X-linked mental retardation associated with terminal X-chromosome constriction" was given the name Martin-Bell Syndrome (Richards et al., 1981), but has become commonly known as Fragile X Syndrome (FXS).

FXS presently affects roughly 1:5000 males and 1:2500-8000 females (Tassone, 2014). This disorder is molecularly defined by a trinucleotide CGG repeat expansion in the 5' untranslated region of the *Fmr1* gene on the X chromosome, identified as the genetic cause in 1991 (Pieretti et al., 1991). The *Fmr1* gene normally contains fewer than 55 CGG repeats, and repeat expansion into a range of 55-200 is considered a premutation allele (Hagerman et al., 2010; Santoro et al., 2012). Premutation carriers are susceptible to Fragile X-Associated Tremor/Ataxia Syndrome, as well as premature ovarian insufficiency in female carriers (Wattendorf and Muenke, 2005). The chance of repeat expansion from a premutation to mutation allele during maternal transmission correlates with the maternal allele size (Fu et al., 1991). An expansion above 200 CGG repeats crosses the full mutation and syndrome threshold, causing transcriptional silencing of *Fmr1* and subsequent loss or reduction of Fragile X mental retardation protein (FMRP). FMRP is a RNA-binding protein that, in the brain, normally represses the translation of key synaptic proteins.

However, *Fmr1* is also expressed throughout the body, and physical manifestations of FXS include elongation of the face; enlargement of the jaw, ears, and testes; and connective tissue abnormalities including mitral valve prolapse and hyperextensible joints (Wattendorf and Muenke, 2005; Tassone, 2014).

FXS is the most common single-gene cause of ASD and intellectual disability, accounting for approximately 2% of ASD cases (Bailey et al., 1993; Wassink et al., 2001; Reddy, 2005). Genomic studies have revealed that a large set of FMRP-associated genes shows high overlap with autism target genes (Iossifov et al., 2012), and that translational regulation by FMRP is important in a variety of molecular pathways that are affected by ASD-related mutations (Parikshak et al., 2013). Of individuals with FXS, 30-60% have autism or an autism spectrum disorder (Harris et al., 2008; Hagerman et al., 2014; Richards et al., 2015), and up to 90% present a notable degree of autistic symptoms (Harris et al., 2008; Wheeler et al., 2015). Accordingly, FXS is particularly compelling as a prototypical neurodevelopmental disorder in which to study circuit mechanisms underlying altered sensory processing.

The neurodevelopmental manifestations of FXS include intellectual disability, language delay, anxiety, and hyperactivity, as well as a number of autistic traits such as social phobia (Butler et al., 1991; Hagerman et al., 1991). The vast majority of FXS patients exhibit some degree of hyperarousal to sensory stimuli and, in particular, tactile defensiveness: an aversion to touch or tactile stimuli, often presenting in children as strong dislike or protest of clothing seams, rough fabrics, touch on the face, or tooth brushing (Butler et al., 1991; Goldsmith et al., 2006). One longitudinal study of sensory dysfunction in boys with FXS between ages 9 months and 60 months found that parent-reported sensory hyporesponsiveness or passivity around ages 9-12 months

tended to precede the emergence of hyperresponsiveness behaviors, and that the latter tended to increase as the child reached preschool age (Baranek et al., 2008). It is certainly possible that infants with FXS might be overwhelmed by sensory stimuli and thus reluctant to interact with their environment, but are also unable to communicate their discomfort. This might result in the apparent passivity at 9-12 months, which then transitions into recognizable hyperresponsiveness as the child becomes more behaviorally mature (Baranek et al., 2008).

EEG studies of sensory processing in humans with FXS have yielded more consistent results than studies of humans with ASD of more varied etiology. At baseline, individuals with FXS have showed decreased alpha power and functional connectivity, with increased theta power and functional connectivity (Sinclair et al., 2016). In addition to acoustic startle tests showing disrupted prepulse inhibition in individuals with FXS, EEG studies in children and adults with FXS have found an increased amplitude of the N1 component of auditory event-related potentials (ERPs), reduced or absent N1 habituation, and increased gamma power with reduced phase-locking (Castren et al., 2003; Van der Molen et al., 2012; Ethridge et al., 2016; Sinclair et al., 2016). These findings suggest differences in both spontaneous and sensory-evoked activity of neocortical circuits involved in sensory processing in FXS.

Circuit-level alterations in the *Fmr1*$^{-/-}$ mouse model of FXS

The detailed study of circuit dysfunction in FXS requires an animal model with a similar phenotype to the human disease. In mice, the *Fmr1* gene, mRNA, amino acid sequence, and protein expression levels are relatively similar to those of the human, providing a biochemical justification

for a mouse with silenced *Fmr1* to model FXS (Bakker et al., 1994). This mouse was originally developed and characterized by the Dutch-Belgian Fragile X Consortium (Bakker et al., 1994). In brief, embryonic stem cells were transfected with a targeting vector containing disrupted murine *Fmr1* DNA. Stem cells with successful homologous recombination were injected into blastocysts, which were then implanted into pseudopregnant female C57BL/6J mice. The chimeric males among the F0 offspring were then crossed to wild-type (WT) females to yield F1 $Fmr1^{+/-}$ females, which were crossed to both WT and chimeric males to yield F2 $Fmr1^{-/-}$ males and females, respectively (Bakker et al., 1994). The initial characterization of these animals noted a loss of the WT *Fmr1* allele, as well as a lack of *Fmr1* mRNA and FMRP (Bakker et al., 1994). A later characterization found that this mouse may not be a true molecular null, and instead does have a low level of residual *Fmr1* mRNA expression and alternatively spliced protein products (Yan et al., 2004; Mientjes et al., 2006). This residual expression may in fact be a useful reflection of molecular variability in humans with FXS, who can have varying residual levels of FMRP due to mosaicism, full or partial methylation status, or X-inactivation in women (de Vries et al., 2003; Jacquemont et al., 2011, 2014).

In humans, repeat instability during oogenesis can lead to expansion from a premutation allele to a full mutation allele, wherein the CGG repeats and *Fmr1* promoter are methylated, causing chromatin condensation and transcriptional silencing (Santoro et al., 2012). Mouse models carrying premutation or mutation-size *Fmr1* alleles have demonstrated repeat instability and repeat expansion; however, even with 230 CGG repeats, these models have failed to show methylation and transcriptional silencing of the *Fmr1* gene (Brouwer et al., 2007; Entezam et al., 2007). As such, the *Fmr1* knockout much more effectively mirrors the loss or near-loss of FMRP seen in FXS.

Despite the differences in molecular pathology between FXS and the *Fmr1*$^{-/-}$ mouse, this mouse is particularly useful for studying the human disease because, in addition to macroorchidism, it exhibits behavioral deficits remarkably analogous to human symptoms. These deficits include deficits in spatial learning, abnormal social behavior, hyperactivity, audiogenic seizures, and increased auditory and air puff startle (**Table 1**) (Bernardet and Crusio, 2006; Contractor et al., 2015; Orefice et al., 2016). Of note, several of the behavioral phenotypes are dependent on the mouse's background strain; for instance, the increased startle responses were described in C57/BL6J *Fmr1*$^{-/-}$ mice (Zhang et al., 2014; Orefice et al., 2016), as was the increased motor stereotypy and marble burying (Spencer et al., 2011), while increased audiogenic seizures are a hallmark of the FVB *Fmr1*$^{-/-}$ mice (Bernardet and Crusio, 2006). EEG and electrophysiological studies in adult mice have also found, similarly to human studies, reduced N1 habituation in auditory cortex and reduced gamma frequency synchrony in the somatosensory cortex (Gibson et al., 2008; Lovelace et al., 2016).

Table 1: Behavioral phenotypes in FXS and *Fmr1*$^{-/-}$ mice

Fragile X Syndrome	*Fmr1*$^{-/-}$ Mouse
Intellectual disability	↓ learning rate, ↓ reversal learning ↓ working memory*
Social anxiety	↓ Passive/receptive social behavior ↑ Nonsocial behavior
Repetitive motor behaviors	↑ Motor perseverance, stereotypy* ↑ Marble burying*
ADHD	↑ Open field activity
Sensory hypersensitivity	↑ Audiogenic seizures* ↑ Auditory, air puff startles*

* Dependent on background strain

The expression of *Fmr1* is developmentally regulated and normally peaks during the second postnatal week in the mouse cortex and the second to fourth postnatal weeks in mouse hippocampus (Meredith et al., 2012). Because this expression timing coincides with critical periods for cortical network development and experience-dependent plasticity, it stands to reason that the loss or reduction of FMRP during development could have massive effects on synaptic and circuit function, both during early development and in adulthood. Indeed, the *Fmr1*$^{-/-}$ mouse shows alterations in activity-dependent synaptic plasticity at P4-7 (Harlow et al., 2010) and delayed pruning of axonal arbors at P14 (Bureau et al., 2008), as well as delayed stabilization and immature morphology of spines at P10-12 and in adulthood (Cruz-Martín et al., 2010; Pan et al., 2010; He and Portera-Cailliau, 2013; Padmashri et al., 2013). In addition, circuit-level studies have found a delay in the developmental GABA polarity switch (He et al., 2014), as well as a delay in the developmental desynchronization of cortical neurons at P14-16 (Gonçalves et al., 2013). It is clear that the *Fmr1*$^{-/-}$ mouse displays a variety of neuronal defects that contribute to delayed circuit maturation (Contractor et al., 2015).

It is still unclear how the many abnormalities in synapses or circuits give rise to specific behavioral and functional abnormalities in the *Fmr1*$^{-/-}$ mouse, just as the pathogenesis of FXS and ASD behavioral deficits remain unparsed. One long-standing hypothesis regarding the pathogenesis of FXS is the *mGluR theory*, based on observations that the *Fmr1*$^{-/-}$ mouse exhibits dysregulated metabotropic glutamate receptor (mGluR) 5-dependent long-term depression (Huber et al., 2000), and that several behavioral and synaptic phenotypes can be rescued by genetic reduction of mGluR or administration of mGluR5 antagonists (Chuang et al., 2005; Yan et al., 2005; Dölen et al., 2007; Michalon et al., 2012). Unfortunately, Phase 2 clinical trials of two mGluR5 antagonists, AFQ056 (mavoglurant) and RG7090 (basimglurant), were discontinued in 2014 because they failed to

demonstrate therapeutic efficacy in adolescents and adults with FXS (FRAXA, 2014; Santarelli, 2014). Another theory of FXS is the *GABA theory*, which argues that *Fmr1*$^{-/-}$ mice show reduced expression of $GABA_A$ receptors, a loss of parvalbumin neurons in neocortex, and reduced tonic inhibition in the amygdala, which cause excess excitability of neurons and may contribute to the anxiety and seizures in children with FXS (D'Hulst and Kooy, 2007; Selby et al., 2007; Pfeiffer and Huber, 2009; Olmos-Serrano et al., 2010). However, a Phase 2 clinical trial of the GABA agonist STX209 (arbaclofen) also failed to demonstrate therapeutic efficacy (Berry-Kravis et al., 2012).

Factors which may have contributed to the lack of clinical trial success include the heterogeneity of patient populations, differences between dosages effective in mice and dosages administered to human subjects, subjects being older than the critical ages for circuit plasticity, a dearth of clear biomarkers for measuring treatment response, and a reliance on parental assessment of symptoms (Mullard, 2015). Improved study design for ongoing and future evaluations of mGluR5 and GABA modulators is certainly necessary. At the same time, these are unlikely to be the only dysregulated pathways in FXS. The development of effective treatments for FXS will certainly require investigation of other pathways that may provide therapeutic targets. Additionally, investigation of how neuronal connectivity is abnormal at the level of circuits and networks in the *Fmr1*$^{-/-}$ mouse can not only fill the gap of understanding between subcellular changes and behavioral deficits in FXS, but can also identify circuit-level biomarkers that could be used to more effectively measure treatment efficacy. These circuit-level phenotypes should also ideally be linked to behavioral phenotypes that more accurately represent functional deficits in humans.

Rationale for the thesis research

Many studies in *Fmr1*$^{-/-}$ mice have revealed increases in neuronal and circuit excitability, including increased intrinsic excitability, reduced inhibition, and network hypersynchrony (Contractor et al., 2015). However, how such hyperexcitability leads to behavioral sensory hypersensitivity, or whether *Fmr1*$^{-/-}$ mice even exhibit an avoidance response to tactile stimuli akin to the sensory overreactivity seen in humans, has not been studied. Moreover, because FXS and ASD present in childhood, circuit and network activity should be studied in young *Fmr1*$^{-/-}$ mice. However, the vast majority of behavioral phenotyping in the *Fmr1*$^{-/-}$ model has used adult animals (Bernardet and Crusio, 2006), potentially because of the technical challenges in performing experiments with young animals. Our lab previously reported that during normal development, layer (L) 2/3 neurons of the mouse barrel cortex, which processes whisker input, show abnormally high network synchrony and spontaneous firing during early development, providing evidence of circuit hyperexcitability during a critical period at postnatal day (P) 14-16 (Gonçalves et al., 2013). We believe that this network hyperexcitability could result in exaggerated neuronal responses to sensory stimuli and contribute to the sensory hypersensitivity symptoms of children with FXS.

I have taken a circuit-to-symptom approach, or rather, a symptom-to-circuit approach, in my studies: beginning with a particular functional deficit in humans with FXS and examining its correlate in the animal model, as well as examining neuronal activity changes that are likely related to the behavioral dysfunction. I tested the hypothesis that specific abnormalities in sensory-evoked network activity in primary somatosensory cortex are associated with tactile defensiveness in *Fmr1*$^{-/-}$ mice. I sought to answer the following questions: do *Fmr1*$^{-/-}$ mice display an impaired behavioral response to whisker stimulation, i.e., an avoidance motor response akin to tactile

defensiveness? What are the circuit-level correlates of sensory hypersensitivity in neocortex that give rise to the tactile defensiveness?

In Chapter 1, I describe our novel behavioral screen for tactile defensiveness in young and adult wild-type (WT) and *Fmr1*$^{-/-}$ mice. In Chapter 2, I describe our novel protocol for expression of the genetically encoded calcium indicator GCaMP6s in early postnatal mice. This protocol enabled our *in vivo* two-photon imaging study of whisker-evoked activity in L2/3 neurons in barrel cortex, described in Chapter 3. Chapter 4 contains a discussion of our findings. Detailed methods are presented at the end of each chapter, along with an appendix describing the statistical approach and considerations.

Chapter **1**

A behavioral assay for tactile defensiveness

The whiskers of rodents enable surface detection, texture discrimination, and navigation (Petersen, 2007). The necessity of whiskers for rodent navigation was conclusively demonstrated over a century ago by Stella Burnham Vincent in her doctoral research (Vincent, 1912). As rodents are nocturnal, relying heavily on somatosensation over visualization (Diamond et al., 2008), Vincent included in her work "a plea for more experimentation involving the cutaneous senses and a protest against the conclusiveness of the analyses of the mental processes of animals when based upon investigations which require the use of the weakest and most defective sense [of vision]" (Vincent, 1912). Whereas humans also use somatosensory inputs derived from contact with hairs on the skin and the skin itself, somatosensation is arguably a weaker sense for many of us, compared with vision and hearing. Nevertheless, the clear phenotype of tactile hypersensitivity and defensiveness in FXS and other ASDs makes it highly relevant to study behavioral responses to tactile stimulation in rodent models of disease.

Because sensory hypersensitivity and tactile defensiveness in FXS and autism present in early childhood, we focused our initial studies on young mice at P14-16. This is a critical period when sensory experience drastically shapes cortical circuits, as mice open their eyes and begin actively whisking (Arakawa and Erzurumlu, 2015). As far as the maturation of brain circuits involved in sensory processing, P14-16 in mice grossly corresponds to the human period between the third trimester and the earliest months of life (Workman et al., 2013).

We first considered whether *Fmr1*$^{-/-}$ mice might display an avoidance response to whisker stimulation that is reminiscent of tactile defensiveness in humans with autism. No previous study has assessed behavioral responses to whisker stimulation at P14-P16; instead, behavioral phenotyping of *Fmr1*$^{-/-}$ mice and other ASD models has relied on adult animals and on assessments

of acute startle response (Bernardet and Crusio, 2006; Orefice et al., 2016; Sinclair et al., 2016). Thus, we developed an assay to detect abnormal behavioral responses to repetitive whisker stimulation (as an aversive tactile stimulus) in head-restrained animals and demonstrated its utility for testing avoidance in both young (P14-16) and adult (P35-41) mice. The animals were awake and head-fixed but able to run freely on a floating polystyrene ball treadmill (**Fig. 1a,** see **Methods**). After a 3 min baseline, we performed a sham stimulation trial during which a flexible wire stimulator was placed in front of the mouse but out of whisker range, to control for any visual startle. The stimulation lasted 80 s and consisted of 20 sequential 1-s stimulations at 10 Hz (anterior-posterior), with a 3 s inter-stimulus interval (ISI). After the sham stimulation, the stimulator was intercalated between whiskers on the left snout, approximately 5 mm from the skin, and the same stimulation protocol was delivered.

Exaggerated motor response to tactile stimulation in 2-week-old *Fmr1*$^{-/-}$ mice

Because of their young age, not all of the P14-16 animals moved on the treadmill (**Fig. 1b**). Despite previous reports of hyperactivity in adult *Fmr1*$^{-/-}$ mice (Bernardet and Crusio, 2006), we did not find a significant difference in the total time spent moving between WT and *Fmr1*$^{-/-}$ mice during the 3 minute baseline period, in the absence of any sham or real (whisker) stimulation (17.1±16.7 s vs. 27.8±18.8 s, respectively; p=0.20 by rank-based two-group comparison with resampling, data not shown). We also did not find increased time running over the 80-second sham or whisker stimulation periods (**Fig. 1c)**. However, we did find that compared to WT mice, a higher proportion of *Fmr1*$^{-/-}$ animals moved during both sham and whisker stimulation conditions

(13/21 during sham stimulation and 15/21 during whisker stimulation, vs. 7/21 and 11/21 for the WT group, **Fig. 1b**). This was the first hint that *Fmr1*$^{-/-}$ mice overreact to tactile stimulation.

We developed this assay under the assumption that in head-fixed mice (both young and adult), increased locomotion might reflect an avoidance response to an aversive stimulus. We hypothesized that young *Fmr1*$^{-/-}$ mice would show increased locomotion only to ongoing real whisker stimulation (as an escape response), whereas the behavior of WT mice would be the same for real and sham stimulation. In other words, WT animals can habituate behaviorally to tactile stimulation, but *Fmr1*$^{-/-}$ mice cannot. As such, we compared locomotion toward the end (last 20 s) of the sham stimulation versus the end of the real whisker stimulation. We found that in WT, the total locomotion time was not different between the two ($p=0.242$ by paired two-group comparison with Bonferroni correction, **Fig. 1d**). In contrast, *Fmr1*$^{-/-}$ animals showed a clear increase in running during the end of the whisker stimulation ($p=0.034$), demonstrating a heightened reaction to the repeated tactile stimulation (**Fig. 1d**).

Figure 1:

Increased locomotion of *Fmr1*$^{-/-}$ mice at P14-16 during repeated whisker stimulation

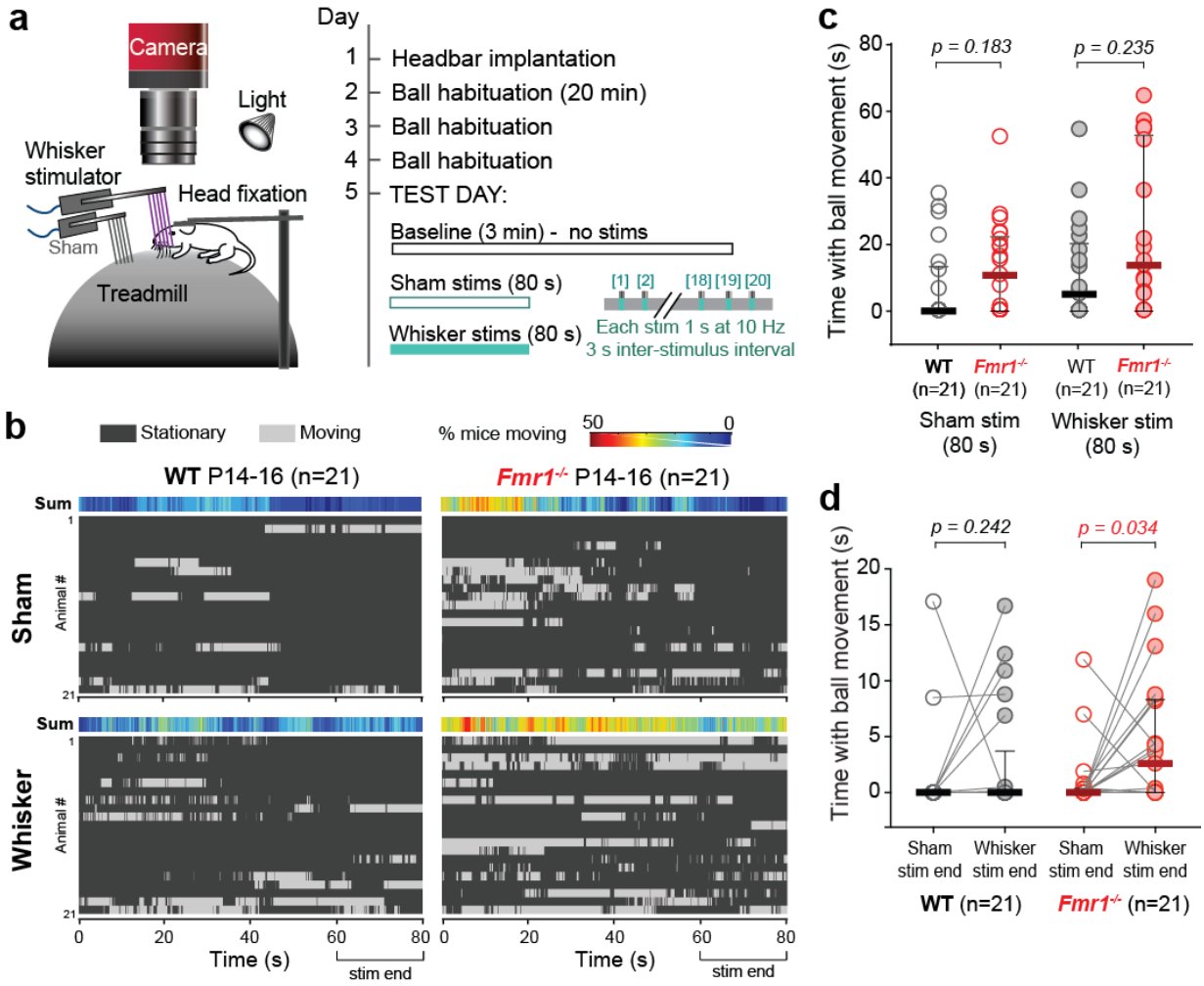

Fig. 1: Increased locomotion of *Fmr1*$^{-/-}$ mice at P14-16 during repeated whisker stimulation

(a) Cartoon of behavioral assay setup (left) and timeline of protocol (right). A whisker stimulator comb of flexible wires, moved by a piezoelectric actuator, was placed in front of but not in contact with the whiskers (sham) or intercalated between whiskers on the left snout (whisker stimulation) as shown.

(b) Locomotion of WT and *Fmr1*$^{-/-}$ mice (n=21 per genotype), postnatal day (P)14-16, during 20 sham and whisker stimulations (each 1 s with 3 s ISI). Each row represents one animal; dark grey means mice were stationary, light grey means they were moving (see Methods). Colored heatmap shows summed running activity across all animals.

(c) Total time spent running during entire 80 s of sham and whisker stimulations, for WT and *Fmr1*$^{-/-}$ mice. In both (c) and (d), circles represent individual mice, bars represent group medians, and error bars represent first/third quartiles. In (c), P-values from unpaired rank-based two-group comparisons with 10,000 resamples and Bonferroni correction.

(d) Total time spent running during last 20 s of sham and whisker stimulations, for WT and *Fmr1*$^{-/-}$ mice. P-values from pairwise rank-based two-group comparisons with 10,000 resamples and Bonferroni correction.

Evidence of tactile defensiveness in adult *Fmr1*$^{-/-}$ mice

Because early postnatal mice have underdeveloped gross motor skills, we could not determine whether increased locomotion on the treadmill represented a true escape response. Thus, we tested whether adult mice manifest a more obvious avoidance response, namely, steering away from the source of aversive stimulation. We used a subset of the mice previously tested at P14-16 and again assayed their behavioral responses to repetitive whisker stimulation at P35-41.

Adult mice showed nearly constant running on the treadmill (**Fig. 2a**), with speeds comparable to those observed in the open field (Niell and Stryker, 2010). The total time running during the sham or whisker stimulations was not different between genotypes ($p=0.41$ and $p=1.00$ by two-group comparisons, **Fig. 2b**). WT animals showed no significant differences in running direction during the entire 80 s of either sham or real whisker stimulation ($p=1.00$ for sham by two-group comparison, $p=0.42$ for real stimulation, **Fig. 2c** left). In contrast, *Fmr1*$^{-/-}$ mice showed significantly more running away from (and less running toward) the stimulator during whisker stimulation ($p=0.005$, **Fig. 2c** left), whereas they showed no directionality during sham ($p=1.000$, **Fig. 2c** right). Hence, adult *Fmr1*$^{-/-}$ mice display a clear avoidance behavior to repeated whisker stimulation, akin to tactile defensiveness.

Figure 2:

Adult *Fmr1*$^{-/-}$ mice show tactile defensiveness during repeated whisker stimulation

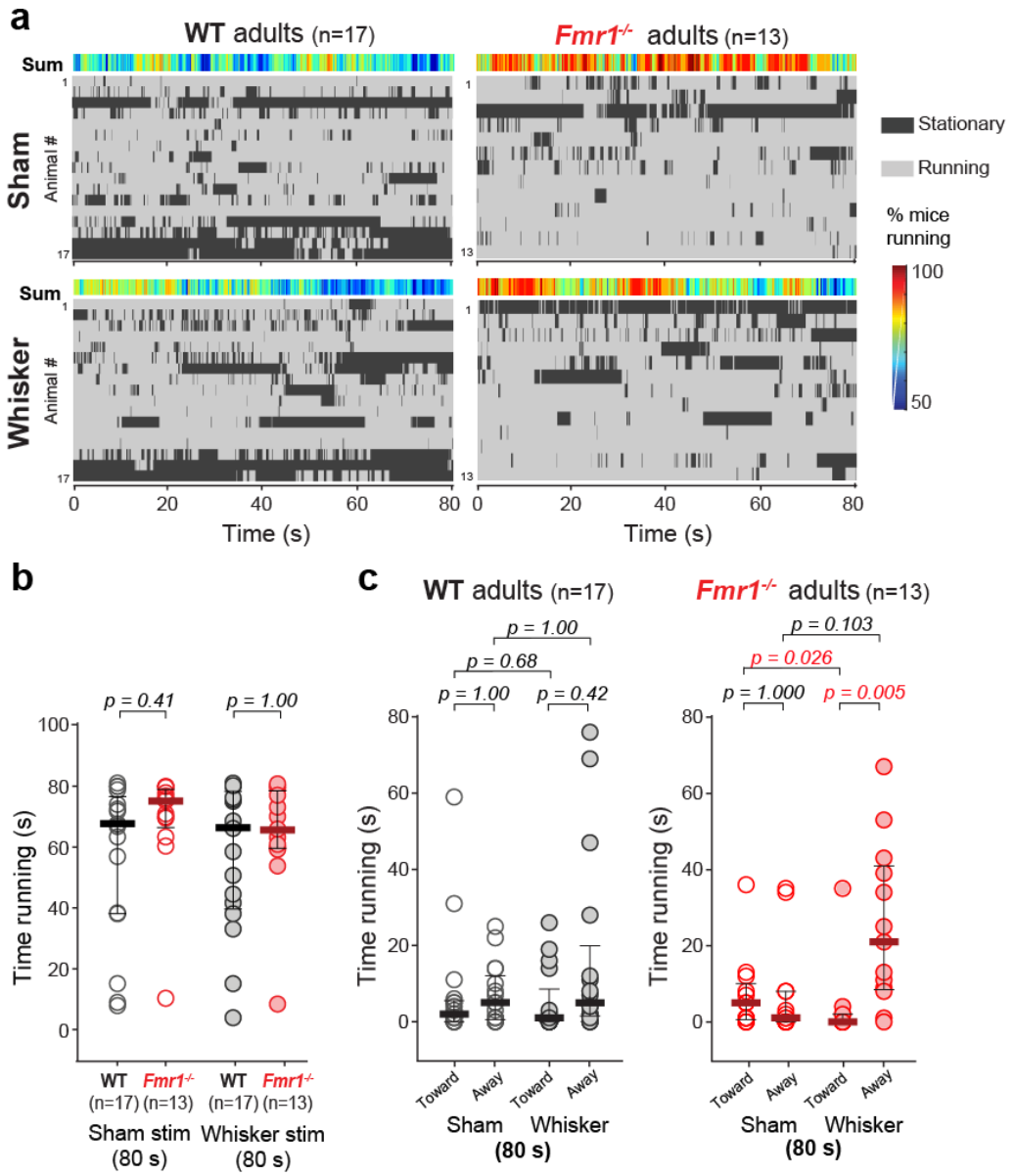

Fig. 2: Adult *Fmr1*$^{-/-}$ mice show tactile defensiveness during repeated whisker stimulation

(a) Running of WT (n=17) and *Fmr1*$^{-/-}$ (n=13) adult mice (P35-41) during repetitive sham and whisker stimulation (as in Fig. 1b).

(b) Total time spent running during entire 80 s of sham and whisker stimulations, for WT and *Fmr1*$^{-/-}$ mice. In (b-d), circles represent individual mice, bars represent group medians, and error bars represent first/third quartiles. In (b), P-values from unpaired rank-based two-group comparisons with 10,000 resamples and Bonferroni correction.

(c) Total time spent running toward (left) or away (right) from whisker stimulator for WT mice during the specified time bins. P-values from pairwise rank-based two-group comparisons with 10,000 resamples and Bonferroni correction.

(d) Total time spent running toward (left) or away (right) from whisker stimulator for *Fmr1*$^{-/-}$ mice during the specified time bins. P-values from pairwise rank-based two-group comparisons with 10,000 resamples and Bonferroni correction.

METHODS

Materials

Unless otherwise noted, materials were purchased from Sigma-Aldrich.

Experimental animals

All experiments followed the U.S. National Institutes of Health guidelines for animal research, under an animal use protocol (ARC #2007-035) approved by the Chancellor's Animal Research Committee and Office for Animal Research Oversight at the University of California, Los Angeles. All experiments used male and female FVB.129P2 WT mice (JAX line 004828) and *Fmr1*$^{-/-}$ mice (JAX line 004624) (Bakker et al., 1994) housed in a vivarium with a 12-h light-dark cycle. Experiments were performed during the light cycle. Animals were weaned at P21-22 and afterward housed with up to five mice per cage. Before P21, pups were housed with their dam. The FVB background was chosen because of its robust breeding, and because the FVB *Fmr1*$^{-/-}$ phenotype includes a predisposition to audiogenic seizures (Bernardet and Crusio, 2006). Due to the potentially stressful effects of surgeries on pups of early prenatal ages and their dams, homozygous litters were used to maximize survival by eliminating the possibility of littermates with different genotypes receiving unequal attention from the dam. Experimenters were aware of

the genotype of the animals in each experiment, as homozygous litters were used. Both male and female animals were used.

Tactile defensiveness assay in head-restrained mice

We adapted the head-restrained paradigm as previously described (Dombeck et al., 2007), where animals are habituated to head restraint on a 200 mm polystyrene ball moving freely on an air cushion within a half-sphere polystyrene shell (Graham Sweet) (**Fig. 1a**). The ball is covered with black dots, 1 cm diameter, hand-drawn with black permanent marker with 2-3 cm between dots. The animal can choose to rest, whisk, or run freely in any direction, with minimal friction. For P14-16 experiments, titanium headbars were implanted at P10-12, and the pups were then habituated on the ball for 20 min/day for three consecutive days, with the earliest age of head restraint being P11 (**Fig. 1a**). Before P11, we observed very little motion from the pups when on the ball. As was previously observed in freely moving pups, not only do neonatal rodents strongly prefer huddling to free exploration in the first postnatal week, they develop exploratory behavior and bilateral whisking at P11-15 (Grant et al., 2012; van der Bourg et al., 2016). For P35-41 experiments, 17 of the WT animals and 13 of the *Fmr1*$^{-/-}$ animals previously tested were re-habituated for four consecutive days before testing.

On the test day, the animal was first placed on the ball for a 3 min baseline period. Next we performed a sham stimulation trial in which the whisker stimulator was visibly moving, but just out of tactile range of the animal's whiskers on its left side (**Fig. 1a**). The stimulator consisted of a long, narrow comb of five slightly flexible wires descending from bent glass capillaries, which

were in turn attached to a piezoelectric actuator. During the stimulation trial, the wires of the stimulator were intercalated between the animal's whiskers. Whisker bundling onto a glass capillary (as used during the imaging experiments) would not have been feasible here because the mouse could have damaged the capillary or unbundled some of its whiskers with its forepaw. The stimulation protocol consisted of a 10 s baseline followed by 20 whisker stimulations along the anterior-posterior direction (1 s long at 10 Hz), with a 3 s ISI, with the stimulations totaling 80 s, ending with another 10 s baseline. This protocol was created based on the fact that mice tend to whisk at 5-15 Hz for bouts of 1-4 s, and is consistent with published studies using a comparable frequency of 8 Hz (Mégevand et al., 2009) and 2-6 s ISI (Kerr et al., 2007; Heiss et al., 2008). A fast infrared camera (Allied Vision Technologies GE680) was used to monitor ball motion and animal movements.

A custom-written semi-automated video analysis routine was implemented in MATLAB to determine when the animal was moving/running vs. stationary (**Fig. 1b and 2a**). The videos were carefully inspected to decide whether the animal was moving forward/backward or left/right (left = toward whisker stimulator, right = away from stimulator) for each one-second increment of video, based on the animal's forelimb movements and the movement of dots on the ball (**Fig. 2c**). Analysis of running during the "end" of the stimulation (**Fig. 1d**) included the last 20 s of the stimulation, which covers the last five stimulations and is a time frame used during later imaging analysis.

Chapter **2**

Neonatal GCaMP injection for imaging of cortical circuit activity during development in awake mice

Fluorescent calcium indicators for imaging neuronal activity

Across cell types and within multiple intracellular compartments, calcium ions (Ca^{2+}) play a variety of roles, including cell cycle regulation, gene transcription modulation, intracellular signaling, and in neurons, neurotransmission (Grienberger and Konnerth, 2012). Action potentials result in massive influxes of Ca^{2+} through voltage-gated channels, as well as the release of Ca^{2+} from intracellular stores (Kandel et al., 2000), and changes in free Ca^{2+} in the presynaptic and postsynaptic compartments contribute to activity-dependent plasticity (Grienberger and Konnerth, 2012). Because the level of intracellular Ca^{2+} is a robust analog for cellular or subcellular responses like action potentials or depolarizations, Ca^{2+} indicators have become powerful tools for visualizing cellular activity in near-real time.

In general, Ca^{2+} imaging relies on a sensor compound that is introduced into neurons (or other cells) and, when bound to Ca^{2+}, changes its fluorescent properties. The two primary classes of Ca^{2+} indicators are the synthetic chemical indicators and the genetically encoded indicators. The chemical indicators (e.g., Fura-2, Indo-1, Fluo-4, Oregon Green BAPTA-1) were pioneered by Roger Tsien's group and utilize a synthetic Ca^{2+} chelator combined with a fluorophore (Grynkiewicz et al., 1985; Tsien et al., 1985; Brain and Bennett, 1997; Gee et al., 2000). When Ca^{2+} binds to the chelator site, the molecule undergoes a conformational change that alters the spectrum of emitted fluorescence (Grienberger and Konnerth, 2012). Fura-2 is excited by ultraviolet wavelengths, produces peak fluorescence at 505-520 nm, and has a relatively fast time course (Tsien et al., 1985). Under two-photon excitation, Fura-2 fluorescence decreases as [Ca^{2+}] increases, making negative fluorescent changes reflective of neuronal activity. In contrast, the fluorescence emitted by Fluo-4 and Oregon Green BAPTA-1 increases above its baseline as [Ca^{2+}]

increases. These chemical Ca^{2+} indicators are typically delivered into single cells via micropipettes (enabling electrophysiology) or electroporation (Grienberger and Konnerth, 2012). Alternatively, a large population of neurons can be bulk-loaded with a cell membrane-permeable acetoxymetyl (AM) ester-conjugated indicator form (e.g., Fura-2-AM or Fluo-4-AM) or dextran-conjugated form, enabling readout of activity across a network (Yuste et al., 2011). While the chemical indicators have high sensitivity and fast on-off kinetics allowing for precise temporal resolution of action potentials, their use must be acute, and they are not amenable for labeling of specific cell populations (Grienberger and Konnerth, 2012).

The genetically encoded Ca^{2+} indicators (GECIs) use, instead of a chelator like BAPTA, a Ca^{2+} binding protein such as calmodulin or troponin. The GECI subcategory of cameleons (Miyawaki et al., 1997), of which Yellow Cameleon is an example (Nagai et al., 2004), utilizes Förster resonance energy transfer (FRET) between two different fluorophores, linked by calmodulin and calmodulin binding peptide M13. Upon calmodulin binding to Ca^{2+}, the conformational change brings the two fluorophores – one ECFP and one Venus – close enough to result in activation of the yellow, resulting in a measurable change in the cyan:yellow fluorescence ratio (Nagai et al., 2004; Grienberger et al., 2014).

Another subcategory of cameleon-based GECIs, the GCaMPs, utilizes a single circularly permuted green fluorophore (GFP), attached to calmodulin and the M13 peptide and maintained in a low fluorescence state when Ca^{2+} is not bound (Nakai et al., 2001). Ca^{2+} binding to calmodulin causes a conformational shift that changes the solvency of the GFP and allows a fluorescence increase (Chen et al., 2013). The earlier GCaMP indicators, GCaMP2 and 3, had relatively low signal-to-noise and slow on-off kinetics. Fortunately, the recent development of the ultrasensitive GCaMP6

has dramatically improved the neuronal event detection capabilities for *in vivo* two-photon imaging in awake, behaving animals; with targeted expression in specific neuronal sub-populations; and with chronic imaging of the same neuronal population (Chen et al., 2013). Single-spike resolution is now possible in sparsely firing neurons, though the off-kinetics of GCaMPs remain slow. Typical expression methods for GECIs include viral transduction (Chen et al., 2013), with the associated limitation of eventual cytotoxicity caused by long-term Ca^{2+} sequestration; and transgenic mice expressing GCaMP (Chen et al., 2012; Zariwala et al., 2012; Dana et al., 2014). Finally, it is important to note that continual improvements have also been made in red-shifted GECIs (Looger and Griesbeck, 2011), with the most recent iterations being jRCaMP1a, jRCaMP1b, and jRGECO1a (Dana et al., 2016).

A new protocol for early postnatal GCaMP expression

The conventional approach for cortical imaging with GCaMP consists of a cranial window surgery with injection of a recombinant adeno-associated virus encoding for the GCaMP into the superficial cortex. Imaging is typically performed 2-4 weeks after surgery (Tian et al., 2009; Chen et al., 2012, 2013; Zariwala et al., 2012). However, injection of rAAV-GCaMP can result in inconsistent expression, with the expression being highest at the injection site but potentially still uneven between nearby cells (Dana et al., 2014), and the progressive viral infection leads to eventual physiological abnormalities and neuronal death starting about four weeks after injection (Tian et al., 2009; Zariwala et al., 2012). These limitations preclude imaging of the same cell population over months. An improvement on injection-based GCaMP expression techniques are

the transgenic mice expressing GCaMP: the *Thy1*-GCaMP3 mice (Chen et al., 2012), the Ai38 mouse with Cre-dependent GCaMP (Zariwala et al., 2012), and most recently, the *Thy1*-GCaMP6 mice (Dana et al., 2014). In particular, the *Thy1*-GCaMP6 line shows higher expression of GCaMP6 and faster kinetics than the GCaMP3 mice, and shows stable expression of GCaMP6 in multiple cortical regions across months (Dana et al., 2014).

However, one of the major drawbacks of existing GCaMP techniques, whether injection-based or in transgenic mice, is the inability to express GCaMP before early adulthood. The Ai38 mouse is treated with tamoxifen at P7 to induce the GCaMP3 expression, and showed very low expression at 4 weeks of age (Zariwala et al., 2012). Because the *Thy1* promoter is developmentally regulated, the *Thy1*-GCaMP2.2 and GCaMP3 mice showed very little expression before 2 months of age (Chen et al., 2012), and the *Thy1*-GCaMP6 mouse also showed sufficient expression for imaging only after 2 months of age (Dana et al., 2014). The injection of rAAV encoding GCaMP is also typically performed at the same time as the cranial window surgery and requires 2-4 weeks between the time of injection and the start of imaging, to allow time for the expression to increase.

Here, I describe a novel protocol for neonatal injection of recombinant AAV encoding GCaMP6s at postnatal day (P) 1, which enables *in vivo* two-photon imaging of L2/3 cortical neurons as early as P10. At P1, a modified burr hole surgery is used to inject the rAAV encoding GCaMP into the desired area of superficial cortex (**Figs. 3-4**), with rapid post-operative recovery of the pup. At P10, a cranial window is implanted over the previously injected area. The pup can be imaged the same day if fully anesthetized, and the next day if lightly sedated or awake. The major advantage of this protocol is that it can be used to chronically image the same population of cells from P10 through adulthood. Of particular note, the GCaMP expression provided by the P1 injection can

enable visualization of the entire process of developmental desynchronization of cortical neurons from P12 through P14, which has never before been shown in the same animal.

Figure 3: P1 injection setup and procedure (drawings by Kim Battista)

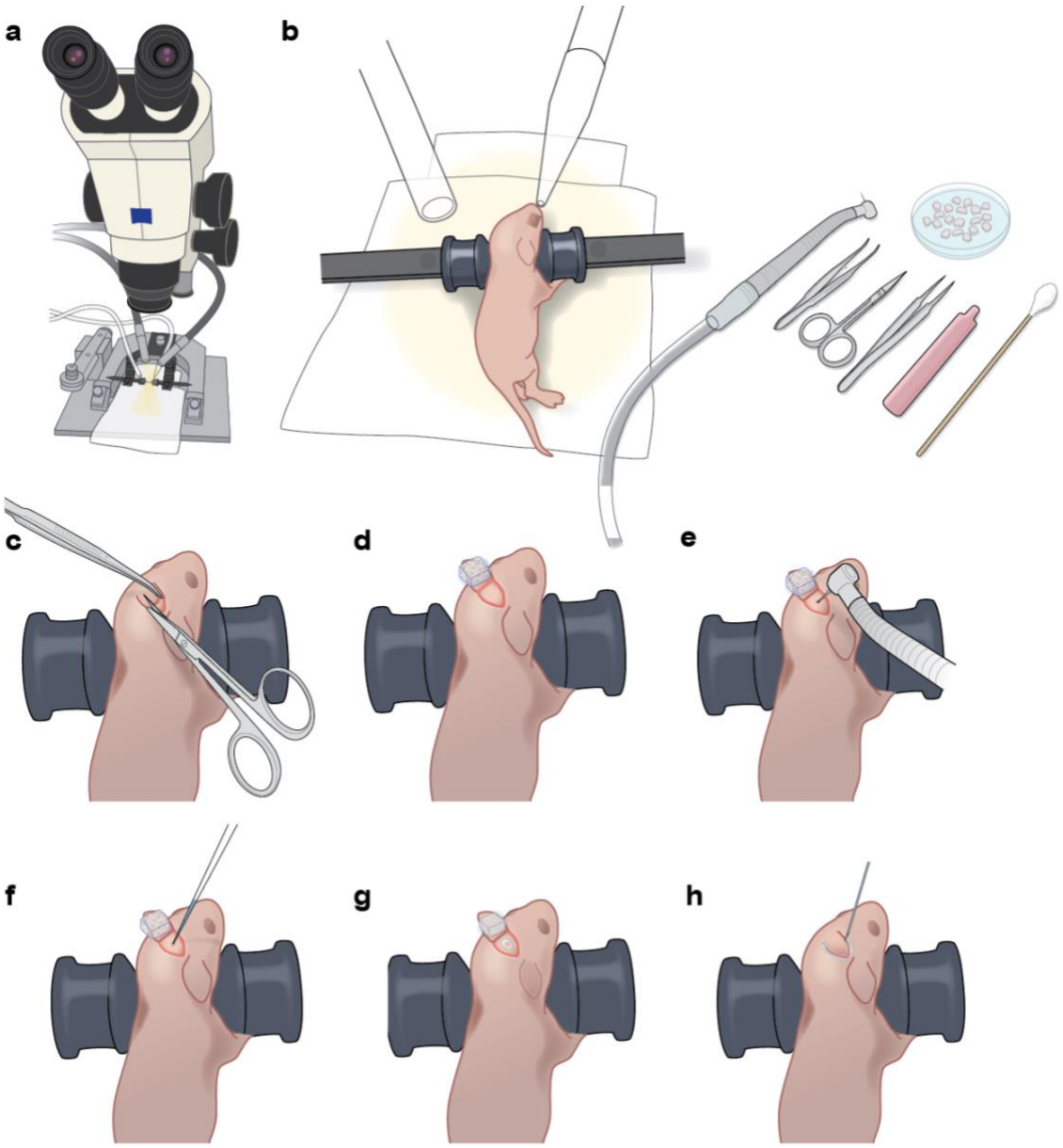

Fig. 3: P1 injection setup and procedure

(a) Dissecting microscope with illumination.

(b) At left, positioning of P1 pup with blunt ear bars, isoflurane delivery next to nose, and exhaust. At right, surgical tools: pneumatic dental drill, forceps, iridectomy scissors, fine forceps, sterile saline vial, sterile cotton swab, and petri dish of Gelfoam soaking in sterile saline.

(c) Creating a 3-4 mm triangular skin flap over the desired injection area.

(d) Folding back the skin flap and covering with wet Gelfoam to prevent the skin flap from drying and shrinking.

(e) Light drilling of exposed skull to crack the bone slightly.

(f) Injection of GCaMP viral vector with glass micropipette.

(g) Sealing of injection site with VetBond.

(h) Sealing of skin flap with VetBond.

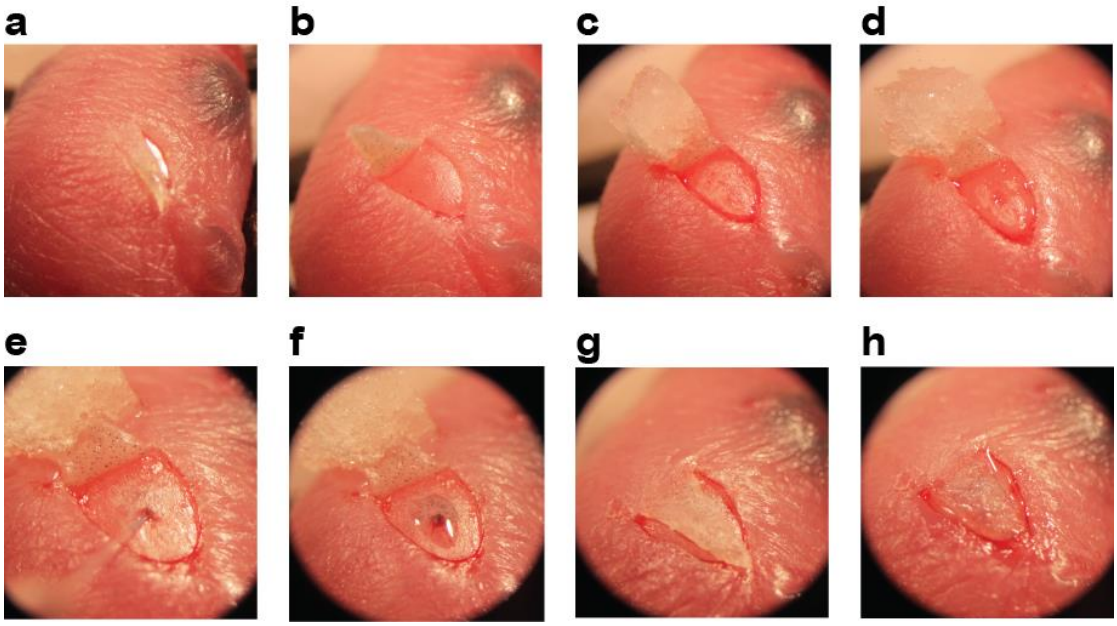

Figure 4: Surgery photographs of P1 injection procedure

(a) Creating a 3-4 mm triangular skin flap over the desired injection area.

(b) Folding back the skin flap and covering with wet Gelfoam to prevent the skin flap from drying and shrinking.

(c) Covering the skin flap with wet Gelfoam to prevent drying and shrinking; exposed skull is dry after light cleaning with dental drill.

(d) Small crack in skull after drilling.

(e) Injection of GCaMP viral vector with glass micropipette.

(f) Sealing of injection site with VetBond.

(g) Replacement of skin flap.

(h) Sealing of skin flap with VetBond.

We have also tested *in utero* injection of rAAV-GCaMP at E15, but observed only scant expression at P6-10, with fewer than 10 cells per imaging field. We believe that overexpression of GCaMP6 in L2/3 progenitor cells causes significant cytotoxicity. The P1 injection is most likely successful because the viral vector infects cells after they have already populated the cortical layers. Postnatal injection is also more versatile and allows for more successful targeting of a specific cortical area (e.g., visual cortex, barrel cortex) than can be easily achieved by *in utero* injection. Confocal fluorescence imaging of cortical slices demonstrated broad expression of GFP in L2/3 neurons (**Fig. 5**).

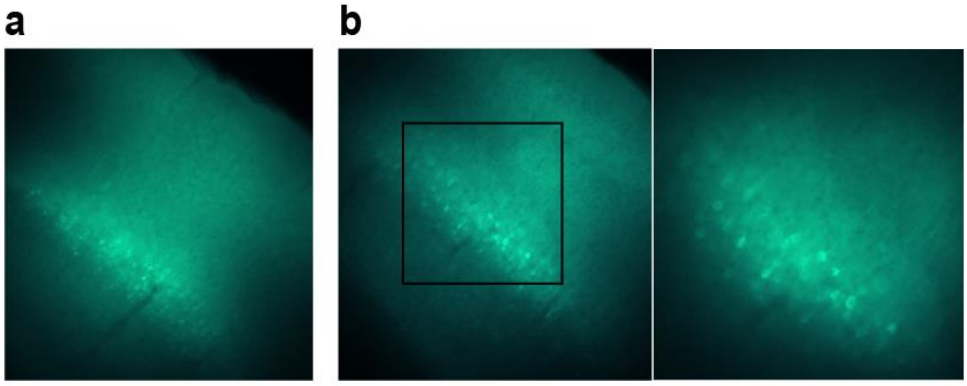

Figure 5: GFP in L2/3 cortex from two P16 animals injected with AAV-GCaMP6s at P1

(a) Fluorescence expression in barrel cortex from a P16 animal after P1 injection. 10X magnification.

(b) Fluorescence expression in barrel cortex from a second P16 animal after P1 injection. 10X magnification at left, with 20X magnification of the boxed area at right.

We also used a brief electrophysiological study to assess the health of neurons expressing GCaMP6s after the P1 injection. We performed whole cell patch-clamp recordings of six L2/3 neurons expressing GCaMP6s in acute slices from two P16-17 pups that had been injected at P1, as well as six L2/3 neurons from two uninjected littermates at the same age, following previously described methods (Goel and Buonomano, 2016). The ACSF solution was consistent between recordings with the exception of the [KCl], which ranged from 1.25 mM to 5 mM. The series resistance varied from 4-7 MΩ during the recordings. The input resistance (R_m) or membrane potential (V_m) did not change more than 15% during the course of recording for each cell. The R_m and V_m were not statistically different between GCaMP-expressing cells (from injected animals) and cells without GCaMP (uninjected animals) **(Fig 6**), demonstrating that the P1 GCaMP expression did not have cytotoxic effects on the neurons.

Figure 6: R_m and V_m of P16-17 L2/3 neurons injected with AAV-GCaMP6s at P1

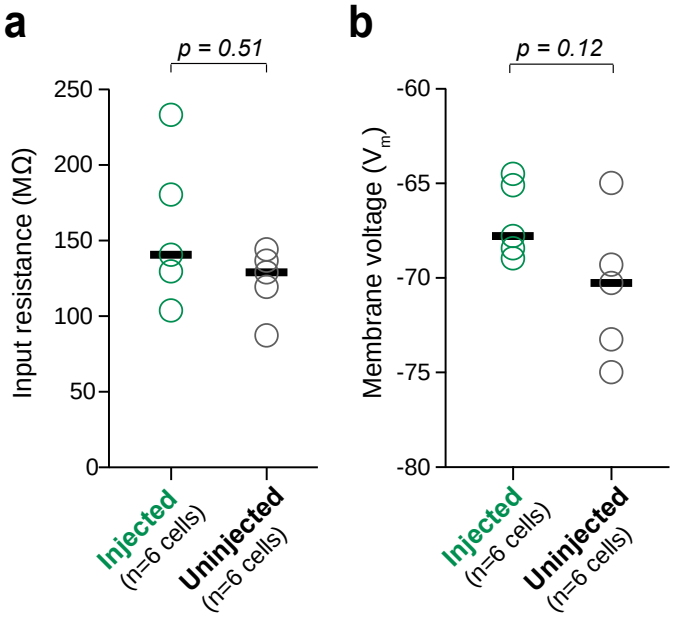

Fig. 6: R_m and V_m of P16-17 L2/3 neurons injected with AAV-GCaMP6s at P1

(a) Input resistance during whole-cell recordings of 6 L2/3 neurons from 2 P16-17 animals injected with AAV-GCaMP6s at P1, and 6 L2/3 neurons from 2 uninjected littermates. For (a-b), each circle represents data for one cell, bars represent group medians, and p-values are from unpaired rank-based two-group comparison with 10,000 resamples.

(b) Membrane voltage during whole-cell recordings of 6 L2/3 neurons from 2 P16-17 animals injected with AAV-GCaMP6s at P1, and 6 L2/3 neurons from 2 uninjected littermates.

There is precedent for the use of neonatal injection of AAV vectors: for example, a P0 intraventricular injection of an AAV vector encoding YFP or Cre-TdTomato has been shown to produce strong expression as early as P2, with levels of expression comparable to adulthood at P7 (Kim et al., 2013). Therefore, we believe that our protocol could be combined with Cre-lox systems for cell type-specific targeting, or even with optogenetic approaches to enable manipulation of circuit activities.

METHODS

The protocol below describes detailed, step-by-step instructions for virus injections in newborn mice that have been optimized for targeting of GCaMP6s in L2/3 neurons of barrel cortex. Adjustments may be necessary for targeting deeper layers or different cortical regions. Additionally, we provide tips for overcoming potential hurdles to this technique (**Table 2**). For example, the P1 injection can cause scarring in the injected area, which can make the subsequent

cranial window surgery much more difficult and reduce experimental efficiency. Scarring can be minimized by the following considerations: 1) a rapid surgical procedure with carefully calibrated anesthesia levels; 2) gentle burr hole drilling that produces only a small crack in the skull through which the glass pipette can be smoothly inserted, ideally without a visible piece of skull being drilled out; and 3) careful application of the minimal amount of VetBond to seal the drilled area and, separately, the skin edges, so that the skull and skin are not glued to each other. If there is scarring, then the subsequent cranial window surgery may be much less successful, reducing the experimental efficiency.

Reagents

All reagents were obtained from Sigma unless otherwise specified.

1. Wild-type or transgenic mice. *Note:* Animal studies must be carried out following institutional and governmental guidelines and regulations.
2. Isoflurane. *Note:* Procedures using isoflurane should be conducted in well-ventilated areas, and should follow relevant animal care guidelines.
3. O_2 tank.
4. Carprofen (Rimadyl, Pfizer, 50 mg/ml)
5. Dexamethasone 2 mg/mL (Fresenius Kabl USA or Henry Schein)
6. Lidocaine HCl 1% + epinephrine 1:100,000 (Hospira)
7. Artificial Tears eye lubricant ophthalmic ointment (Henry Schein)
8. Sterile NaCl (Addipak)
9. AAV vector encoding GCaMP (U. Penn virus core), diluted to 2e13 concentration with 1% Fast Green

10. 70% ethanol
11. Betadine (Purdue Products)
12. Sterile Gelfoam (absorbable gelatin sponge) (Ethicon)
13. Cyanoacrylate glue (Krazy Glue)
14. Ortho-Jet dental acrylic (Lang Dental)

Equipment (**Fig. 3a-b**)

1. Capillary puller (Narashige)
2. Glass capillaries, O.D. 1.5 mm, I.D. 0.86 mm (Sutter Instruments)
3. Picospritzer injection device (Parker Hannifin)
4. Glass bead sterilizer (Fine Science Tools)
5. Water recirculating heating blanket (Stryker) and pump (Gaymar)
6. Rodent trimmer (Wahl)
7. Dissecting microscope (Zeiss)
8. Stereotaxic frame (Kopf)
9. Anesthetic vaporizer (e.g. Surgivet Classic T3) with airflow meter (Porter)
10. Pneumatic dental drill with drill bits (Henry Schein)
11. Forceps, iridectomy scissors (World Precision Instruments)
12. Small petri dish (e.g. 35-mm diameter)
13. Sterile cotton swabs (Henry Schein)
14. Glass coverslips, 5 mm (Electron Microscopy Sciences)
15. Titanium or aluminum head bars (custom)
16. 2P laser scanning microscope

17. Tunable Ti:Sapphire pulsing laser (Chameleon, Coherent)
18. Objectives (4x and 20x water immersion)
19. Resonant scanning mirrors, amplifiers and PMTs
20. Image acquisition software (we used ScanImage (Pologruto et al., 2003))

Equipment setup (**Fig. 3b**)

1. Pipette preparation for injection: Pull a custom micropipette from a 1.5-mm outer diameter (o.d.), 0.86-mm inner diameter glass capillary tube so that the length of the tapered tip is approximately 8 mm. Break pipette tip slightly by gently touching the tip to the side of sterilized forceps. The o.d. of the tip should be 12.5-25 um. If the tip is too wide, the viral vector may reflux around the needle during the injection.
2. Gelfoam preparation: Use sterilized scissors to cut small pieces of Gelfoam, approx. 1 mm on each side. Soak them in a small petri dish filled with sterile saline.
3. Surgical instruments: Sterilize instruments in a glass bead sterilizer and spray with ethanol before use.
4. Heating blanket: Turn on heating blanket 15 minutes before start of each surgical procedure so that blanket temperature is sufficiently high once mouse is anesthetized.

P1 burr hole injection procedure (timing 15-20 min):

1. *Preoperative care:* Administer subcutaneous injection of carprofen (5 mg/kg BW) to the mouse.
2. Anesthetize the mouse with 5% isoflurane for induction, followed by 2% isoflurane for maintenance.

3. Use blunt ear bars to position mouse so that desired injection area is as flat as possible, with isoflurane delivery over nose (**Fig. 3b**). Ensure that the mouse remains warm (on the heating pad) throughout the procedure, and monitor breathing carefully, including tail and toe pinches. Young pups will tend to breathe erratically, making close monitoring under anesthesia crucial. The ear bars should prevent movement of the pup during subsequent manipulations, without applying excessive pressure to the soft skull. Ensure that the heating blanket is functioning correctly.
4. Sterilize operating area using three alternating wipes of betadine and 70% alcohol.
5. Using the iridectomy scissors, make one snip to create a 3-4 mm triangular skin flap over the desired injection area (**Figs. 3c, 4a**). Fold back the skin flap and cover with a piece of wet Gelfoam to prevent the skin from drying and shrinking (**Figs. 3d, 4b-c**).
6. Immediately apply a drop of lidocaine/epinephrine. After 30 seconds, dry surface.
7. Use pneumatic dental drill and repeated light touches of the drill bit tip to clear the periosteum from the skull surface. Use wet Gelfoam to clean the area of foam and debris, then let the area dry. At this step, the drill bit should not touch the skull surface.
8. Once the exposed skull is clear of periosteum and dry, apply repeated light touches of the drill bit tip at the desired injection site until the bone has clearly weakened and very slightly cracked, enough to permit insertion of the glass micropipette (**Figs. 3e, 4d**). Clean up any bleeding with Gelfoam. Ideally, there should be no bleeding and no visible removal of a piece of skull. If any bone is visibly removed by the drilling, that will delay healing and result in a larger scar, which will make the later cranial window surgery less successful.
9. Load glass micropipette with approximately 200 nL of GCaMP viral vector and position for injection at 45^{o} angle to skull surface.

10. Lower pipette until pipette tip has pierced through the cracked bone and into superficial cortex (**Figs. 3f, 4e**). Inject vector using the picospritzer. Withdraw pipette. *Note:* if the pipette tip is sufficiently narrow, the vector should not reflux.
11. Using a needle tip (e.g., 19-gauge), apply a very small drop of VetBond to the injection site (just enough to seal the cracked area but not enough to reach the skin edges) and let dry completely (**Figs. 3g, 4f**).
12. Replace the skin flap and seal the skin edges with a minimal amount of VetBond (**Figs. 3g, 4g-h**).
13. Allow VetBond to dry before placing mouse in warm recovery cage. After the mouse completely recovers from anesthesia, return it to the litter. Carefully monitor the dam and the pups to ensure reintegration of the post-operative pup(s). Minimize rearrangements of the litter in the cage to reduce stress on the dam and reduce the possibility of cannibalism. Placing a small cardboard shed in the cage can also reduce stress for the dam.

P10-P13 cranial window procedure (timing 45 min – 1 hr) (technique based on Cruz-Martín et al., 2010; Holtmaat et al., 2012)

1. Anesthetize the mouse with 5% isoflurane for induction, followed by 1.5-2% isoflurane for maintenance. Monitor anesthesia level throughout surgery by watching breathing, as well as using tail and toe pinches, and ensure that heating blanket is functioning correctly.
2. Use rodent trimmer to shave from the neck to the eyes, being careful not to trim any whiskers.
3. Use blunt ear bars to position mouse on stereotaxic frame, with anesthesia nose cone. The ear bars must be secured with just enough pressure such that the mouse's head does not

shift during surgery. The skull is still soft at P10 and care must be taken not to excessively squeeze the skull between the bars.

4. Administer subcutaneous injections of carprofen (5 mg/kg BW) and dexamethasone (0.2 mg/kg BW).
5. The original injection site should be apparent as a triangular scar on the skin, not raised or inflamed. If a large plug of fibrous tissue is present at the original injection site, and the skin at the injection site cannot be freely moved above the skull, there is likely an excessive amount of scarring that will preclude a successful window surgery.
6. Sterilize operating area using three alternating wipes of betadine and 70% alcohol.
7. Using the scissors, remove the skin on top of the skull, as well as the periosteum. Apply lidocaine/epinephrine to skin edges. After 30 seconds, dry skull surface using cotton swabs.
8. Apply a small amount of cyanoacrylate glue to the skin edges, but do not apply glue on top of sutures.
9. Use a pneumatic dental drill to very lightly trace a circular window of 3-4 mm in diameter. Apply lidocaine/epinephrine, let sit for 30 seconds, then dry skull. The skull at P10 is still very soft, and the bone near the injected area will also be particularly brittle. Drilling should proceed with minimal pressure to reduce the chance of excessive bleeding.
10. Continue to gently drill along circular trace until bone has been weakened all around the craniotomy. When the center of the craniotomy is pushed gently, it should indent slightly. Clean up any bleeding with Gelfoam.
11. Apply a drop of saline, let sit for up to 10 min. Then use fine-tipped forceps to gently lift the craniotomy. Apply Gelfoam to stop any minor bleeding. Also use Gelfoam to wipe

away any scar tissue remaining from the original burr hole and injection. Minimal bleeding at the edge of the window, if readily staunched with Gelfoam, should not impede imaging that same day. However, bleeding, bruising, or damage to the dura in the center of the window will preclude same-day imaging and, if severe, may also preclude later imaging. Remove bone dust using sterile saline irrigation and Gelfoam.

12. Apply a small drop of saline to keep brain moist, then position a glass coverslip onto the dura.
13. Hold coverslip in position using forceps, with gentle pressure so that coverslip is resting against the bone edges. With the other hand, apply small drops of cyanoacrylate to the coverslip edge at two or three points, securing the coverslip to the skull. Cyanoacrylate should not seep onto the dura. Let cyanoacrylate dry completely.
14. Mix dental acrylic and apply over the entire skull surface, also sealing the edges of the coverslip. Use acrylic to secure headbar to the caudal edge of the acrylic area, so it will not impede the mouse's feeding or the positioning of the microscope objective. The plane of the headbar should be parallel to the coverslip. Also use dental acrylic to make a small well around the window to hold water for the 20X immersion objective.
15. Allow the dental acrylic to cure for 5-10 minutes, and then move mouse to a warm recovery cage. When the mouse has recovered from anesthesia completely, return to the litter. Monitor the dam closely to ensure the pups are reintegrated. Placing a cardboard shed in the cage can improve the dam's caretaking of pups.
16. The mouse can be imaged later the same day if re-anesthetized and maintained under anesthesia during imaging, to prevent any movement that might damage the window before

the dental acrylic is completely cured. If imaged the same day, the session should be brief to minimize the total duration of anesthesia exposure.

Table 2: Troubleshooting for P1 injection and P10-13 cranial window

Problem	Possible reason	Solution
Mouse is moving	Insufficient anesthesia	1. Check that isoflurane delivery is immediately adjacent to or covering the nose. 2. Check that ear bars are not too tight. 3. Increase maintenance anesthesia to 2.5% 4. If mouse is still moving, remove the mouse from the stereotax and re-induce at 5%, then reposition on stereotax.
Mouse dies during surgery	Excessive anesthesia, hypothermia, or excessive cranial pressure.	1. Keep duration of surgery (anesthesia time) under 20 minutes. 2. Adjust isoflurane level to ensure that mouse is still breathing regularly, though slowly, during surgery, and without response to toe or tail pinches. 3. Ensure that heating blanket temperature is sufficiently high. 4. Check that ear bars are not too tight. Skull should be immobile but only barely bulging between the ear bars.
Bleeding during drilling	Damaged blood vessels, or the drill bit punctured the dura.	1. Apply wet Gelfoam to the drilled area and let sit for 30 seconds. If bleeding stops, then proceed with surgery. If bleeding does not stop, irrigate with sterile saline and then apply wet Gelfoam. 2. If the drill bit has clearly punctured through the skull and into the dura, terminate the surgery.
Vector does not exit the pipette tip	The pipette is clogged	1. Increase the picospritzer pulse duration and apply a single larger pulse of pressure to try and unclog the pipette, then proceeding with the injection at lower duration. 2. If the pipette tip remains clogged, retract the pipette and switch to a new pipette.

Vector refluxes around pipette tip and pools on skull	The pipette tip is too wide	1. Use barely any pressure to break the pipette tip. 2. Reduce the picospritzer pulse duration and increase the pause time between pulses (i.e. reduce the volume injected per pulse), to allow time for the injected vector to absorb away from the pipette tip. 3. After injection is complete and the pipette is retracted, use wet Gelfoam to thoroughly clean the skull surface before applying VetBond.
Skin at injection site has adhered to the skull (excessive scarring)	Removal of too much bone, excessive VetBond application, or skin flap replacement before VetBond on skull was dry	1. If the skin at the injection site is adhered to the skull, it is possible that the cranial window can still be completed (i.e. the dura and skull may not be adhesed). 2. If the skull flap cannot be lifted due to adhesion, terminate the surgery.
Bleeding occurs upon bone flap removal	Blood vessel damage or dura damage	1. Apply wet Gelfoam to the drilled area and let sit for 30 seconds. If bleeding stops, then proceed with surgery. If bleeding does not stop, irrigate with sterile saline and then apply wet Gelfoam. 2. If the drill bit has clearly punctured through the skull and into the dura, or if the bone flap has ripped the dura, terminate the surgery.

Chapter **3**

In vivo imaging of local network activity in L2/3 of barrel cortex

The elucidation of the neurobiological pathway for whisker processing began in 1970, with Thomas Woolsey and Hendrik van der Loos' description of "multicellular cytoarchitectonic units – ranging from about 100 μm to 400 μm – which [they] termed 'barrel[s]'" in Layer 4 of the mouse somatosensory cortex (Woolsey and van der Loos, 1970). The primary vibrissal somatosensory (barrel) cortex was uniquely suited to our investigation of circuit-level sensory activity because of the well-defined somatotopy between the anatomical barrel map and the whisker pad: inputs from individual whiskers are progressively processed by specific barrelettes in the trigeminal nucleus, barreloids in the thalamus, and eventually the L4 neurons in barrel cortex (Petersen, 2007). L2/3 pyramidal neurons function in early intracortical processing and provide outputs from the barrel cortex, and while the barrel map remains intact, L2/3 neurons show much greater heterogeneity of responses compared with L4 (Sato et al., 2007; O'Connor et al., 2010; Kuhlman et al., 2014).

Prior studies using single-cell electrophysiological approaches to characterize L2/3 neurons in barrel cortex have shown sparse coding of whisker inputs, with neurons firing on average one action potential per whisker deflection (Sato et al., 2007; Heiss et al., 2008; Mégevand et al., 2009; Sachidhanandam et al., 2013). More recent work utilizing the calcium indicators Oregon Green BAPTA-1 (Kerr et al., 2007; Clancy et al., 2015) or GCaMP3 (O'Connor et al., 2010) revealed that many L2/3 neurons show no response to whisker stimulation (Sato et al., 2007; O'Connor et al., 2010); in fact, only 25% of excitatory neurons in a single imaging field show responses tuned to the anatomically associated whisker (Clancy et al., 2015). The newer and more sensitive calcium indicator GCaMP6s (Chen et al., 2013) enabled confirmation, with greater sensitivity, of the heterogeneity of L2/3 neuronal responses (Peron et al., 2015).

A reduced fraction of L2/3 neurons in barrel cortex respond to whisker stimulation in P14-16 *Fmr1*$^{-/-}$ mice

In light of the maladaptive whisker-induced behavioral responses that are already present in young *Fmr1*$^{-/-}$ mice, described in Chapter 1, we considered the underlying cortical circuit alterations in early postnatal development. P14-P16 is a critical period in sensory processing because the pattern of neuronal activity in barrel and visual cortices has just undergone a marked transition from high synchrony to a decorrelated and more computationally efficient state (Golshani et al., 2009; Rochefort et al., 2009; Frye and MacLean, 2016; O'Donnell et al., 2017). We tested three possible cortical mechanisms underlying sensory hypersensitivity in *Fmr1*$^{-/-}$ mice: 1) Neurons exhibit higher-than-normal firing rates in response to sensory stimulation; 2) A higher proportion of neurons respond to stimulation; and 3) Neurons show reduced adaptation (desensitization) to repetitive sensory stimuli. We considered the last possibility especially likely, based on the lack of behavioral adaptation to whisker stimulation we observed in *Fmr1*$^{-/-}$ mice.

To record whisker-evoked activity in L2/3 neurons of the barrel cortex, we used *in vivo* two-photon imaging of GCaMP6s signals (Chen et al., 2013) in P14-16 mice. First, we injected AAV1.Syn.GCaMP6s.WPRE.SV40 at P1, as described in Chapter 2, and then implanted a glass-covered cranial window at P10-12; we confirmed our targeting of barrel cortex with optical intrinsic signal imaging at P12-15 (see **Methods**, **Fig. 7a-c**). During imaging the animals were head-fixed, awake, and lightly sedated with isoflurane (<0.5%) and chlorprothixene. We first recorded spontaneous activity (205 s), followed by whisker-evoked activity (103 s), for which the animals received the same stimulation direction, timing and frequency as during the behavioral experiments (**Fig. 7d-e**). We did not find significant differences between WT and *Fmr1*$^{-/-}$ mice

in equivalent periods of spontaneous or whisker-evoked activity (Spontaneous: median fluorescence Z-score ± median absolute deviation was 4.73±0.43 for WT vs. 3.85±0.98 for *Fmr1*$^{-/-}$, p=0.31 by two-group comparison; Evoked: 3.13±0.39 for WT vs. 3.14±0.74 for *Fmr1*$^{-/-}$, p=1.00, **Fig. 7f**).

Next, we asked whether whisker stimulation recruits a larger-than-normal cohort of barrel cortex neurons in *Fmr1*$^{-/-}$ mice. To do so, we calculated the proportion of L2/3 neurons that responded to whisker stimulation in a time-locked fashion (see **Methods, Fig. 7g**). Unexpectedly, we found that nearly half (45%) as many neurons exhibited an activity pattern that was time-locked to epochs of whisker stimulation in *Fmr1*$^{-/-}$ compared to WT mice (37.2±9.1% of WT neurons vs. 20.5±13.0% of *Fmr1*$^{-/-}$ neurons; p=0.022 by two-group comparison, **Fig. 7h**). This suggests that the behavioral overreactivity that *Fmr1*$^{-/-}$ mice manifest is not due to either exaggerated sensory-evoked firing of local networks in barrel cortex or to higher proportions of neurons within local networks being recruited by whisker stimulation.

Figure 7: Differences in whisker-evoked network activity in *Fmr1*$^{-/-}$ mice at P14-16

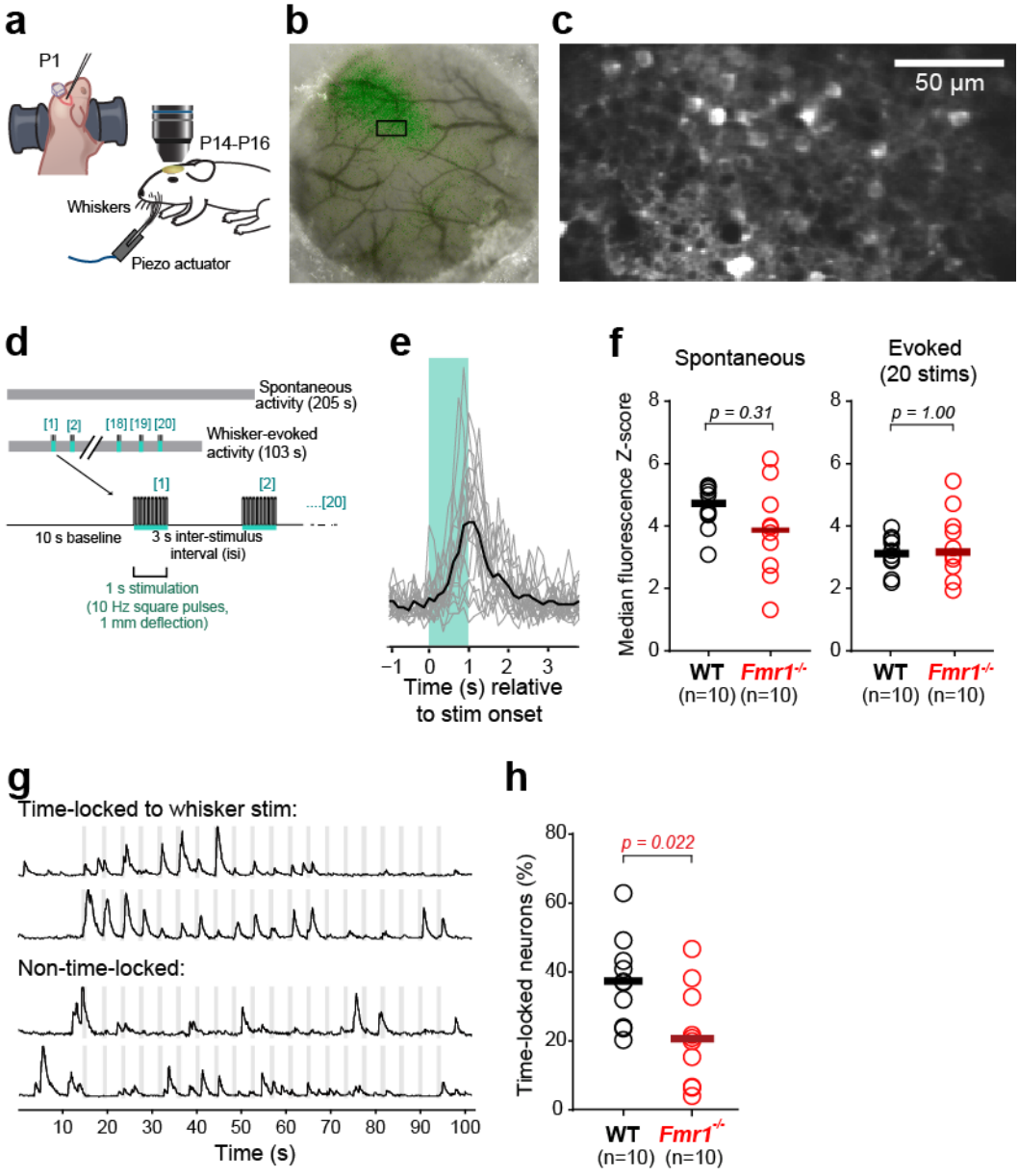

Fig. 7: Differences in whisker-evoked network activity in *Fmr1*$^{-/-}$ mice at P14-16

(a) Schematic of how AAV vector for GCaMP6s injection was injected into somatosensory cortex at P1 (*left*), and P14-16 *in vivo* imaging and whisker stimulation setup (*right*).

(b) Example cranial window over right somatosensory cortex at P14 and a map of whisker-evoked activity obtained with optical intrinsic signal imaging (green). Black box shows location of *in vivo* calcium imaging in (c).

(c) Example field of view of neurons expressing GCaMP6s in the same mouse (at P15) shown in (b) at P15 (xyt SUM projection of 100 consecutive frames at 7.8 Hz).

(d) Protocol for recording spontaneous (1600 frames ≈ 205 s) and whisker-evoked activity (800 frames ≈ 103 s).

(e) Example of individual fluorescent signals extracted from one L2/3 neuron during 20 whisker stimulations (grey) and the mean signal (black).

(f) Median fluorescence Z-scores for spontaneous (left) and whisker-evoked activity (right) of L2/3 neurons in WT and *Fmr1*$^{-/-}$ mice at P14-16 (n= 10 mice per genotype). Each circle shows the median Z-score across all ROIs for one animal, for equivalent durations of spontaneous and evoked imaging (103 s). Bars represent group medians. In panels (f) and (h), p-values from two-group rank-based comparisons with 10,000 resamples, and Bonferroni correction in (f).

(g) Example fluorescence traces from two L2/3 neurons with activity that is time-locked (*top*) and from two different neurons with activity that is not time-locked (*bottom*) to whisker stimulation epochs (light grey bars).

(h) Local networks in *Fmr1*$^{-/-}$ animals have 50% fewer time-locked cells compared with WT.

To determine whether the structure of sensory-evoked network activity differs between WT and *Fmr1*$^{-/-}$ mice, we also compared the timing of peak activity relative to the onset of whisker stimulation. After sorting all whisker-responsive cells by the timing of their peak extrapolated firing rate relative to the stimulation onset, we did not find a difference in the two genotypes' temporal distributions (**Fig. 8**). At the spatial (~1 barrel) and temporal (~125 ms/bin) scales we examined, sensory-evoked activity propagates at comparable rates in WT and *Fmr1*$^{-/-}$ barrel cortex.

Figure 8: Propagation of whisker-evoked activity across local networks at P14-16

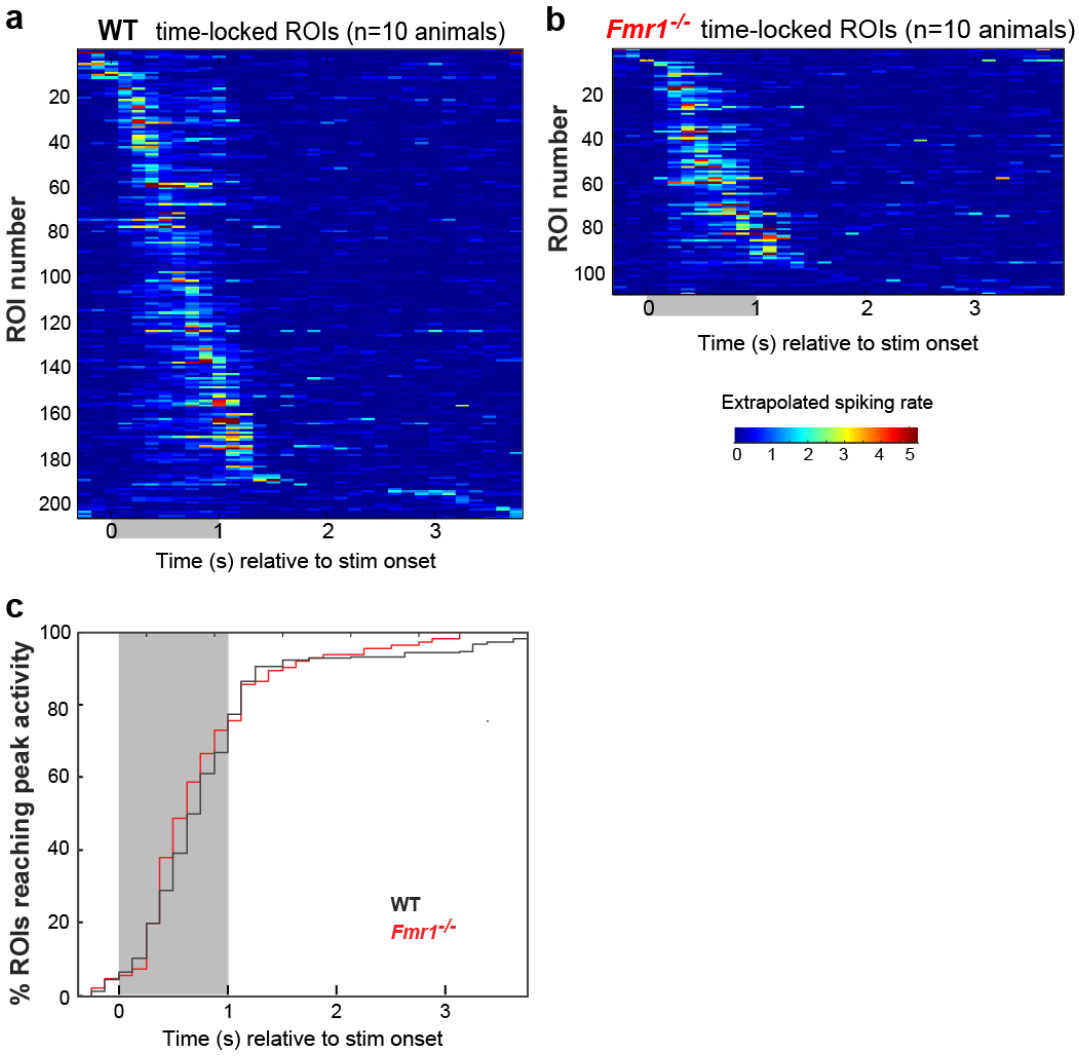

Fig. 8: Propagation of whisker-evoked activity across local networks at P14-16

(a) Heatmap of activity for all time-locked ROIs in WT (n=208 cells). After conversion of fluorescence Z-scores into extrapolated spiking rates (see Methods), spiking rates for each ROI were averaged across all 20 stimulation time bins (from 0.2 s before each stimulation onset to 2.8 s after stimulation end). ROIs were sorted and activity was plotted based on timing of their peak extrapolated spiking rate.

(b) Heatmap of activity for all time-locked ROIs in *Fmr1*$^{-/-}$ mice (n=111 cells), sorted as in (a).

(c) Cumulative histogram showing the % of ROIs in WT and *Fmr1*$^{-/-}$ mice reaching peak activity at different times relative to the stimulation onset.

Impaired adaptation of local whisker-evoked neuronal activity in P14-16 *Fmr1*$^{-/-}$ mice

Our experimental design allowed us to determine whether L2/3 neurons exhibit any adaptation during the 20 sequential whisker deflections, i.e., a reduction in firing with successive stimulations. We found that some L2/3 neurons showed robust adaptation, while others did not (**Fig. 9a-b**). When we analyzed whisker-evoked activity of all neurons imaged in each P14-16 WT animal, we found that the decrease in activity over time could be fit by an exponential curve with a decay constant τ=4.1±1.3 stimulations (**Fig. 9c**). Accordingly, we compared neuronal activity during the first five stimulations with activity during the last five stimulations. This analysis revealed that in WT mice at P14-P16, neuronal activity was significantly lower during the last five stimulations than during the first five (Z-scores: 3.56±0.27 vs. 2.02±0.38, p=0.028 by two-group comparison, **Fig. 9d**). In sharp contrast to WT mice, however, there was no significant change for *Fmr1*$^{-/-}$ mice in neuronal activity from the first five to last five stimulations (2.95±1.01 vs. 2.59±0.99, p=1.000, **Fig. 9d**), suggesting that neural circuits in the mutant mice are unable to adapt to repetitive tactile stimuli.

We then wondered whether neuronal adaptation might only be evident in cells that responded to whisker stimulation in a time-locked fashion. The subpopulation of time-locked cells showed robust adaptation in both WT and *Fmr1*$^{-/-}$ mice at P14-16 (WT p=0.011 by two-group comparison; *Fmr1*$^{-/-}$ p=0.005, **Fig. 9e** left). Interestingly, while non-time-locked cells also showed significant adaptation in WT mice, they did not in *Fmr1*$^{-/-}$ mice (WT p=0.018; *Fmr1*$^{-/-}$ p=1.000, **Fig. 9e** right). It appears that the lack of modulation of the activity of non-time-locked cells in the young *Fmr1*$^{-/-}$ mice contributes to the defect in overall network adaptation during repetitive whisker stimulation. As a control for possible effects of continuous calcium imaging, we analyzed spontaneous activity

of all ROIs during the equivalent "first five" and "last five" time bins, and found no significant change within either genotype (**Fig. 9f**).

Finally, we analyzed the correlation between the WT and *Fmr1*$^{-/-}$ animals' proportions of time-locked neurons and the degree of neuronal adaptation, calculated as an Adaptation Index:

$$\frac{(Z\ score\ during\ First\ 5\ stimulations) - (Z\ score\ during\ Last\ 5\ stimulations)}{(Z\ score\ during\ First\ 5\ stimulations) + (Z\ score\ during\ Last\ 5\ stimulations)}$$

In WT mice, these two measures were significantly correlated (Spearman's ρ=0.733, p=0.021 by bootstrapping with 10,000 resamples) (**Fig. 9g**). In *Fmr1*$^{-/-}$ mice, these two measures were not correlated (Spearman's ρ=0.273, p=0.436) (**Fig. 9g**). This finding indicates that the defect in L2/3 neuronal adaptation in the *Fmr1*$^{-/-}$ mice is linked to their reduced proportion of time-locked neurons in local networks.

Figure 9:
Lack of adaptation of whisker-evoked activity in local networks of P14-16 *Fmr1*$^{-/-}$ mice

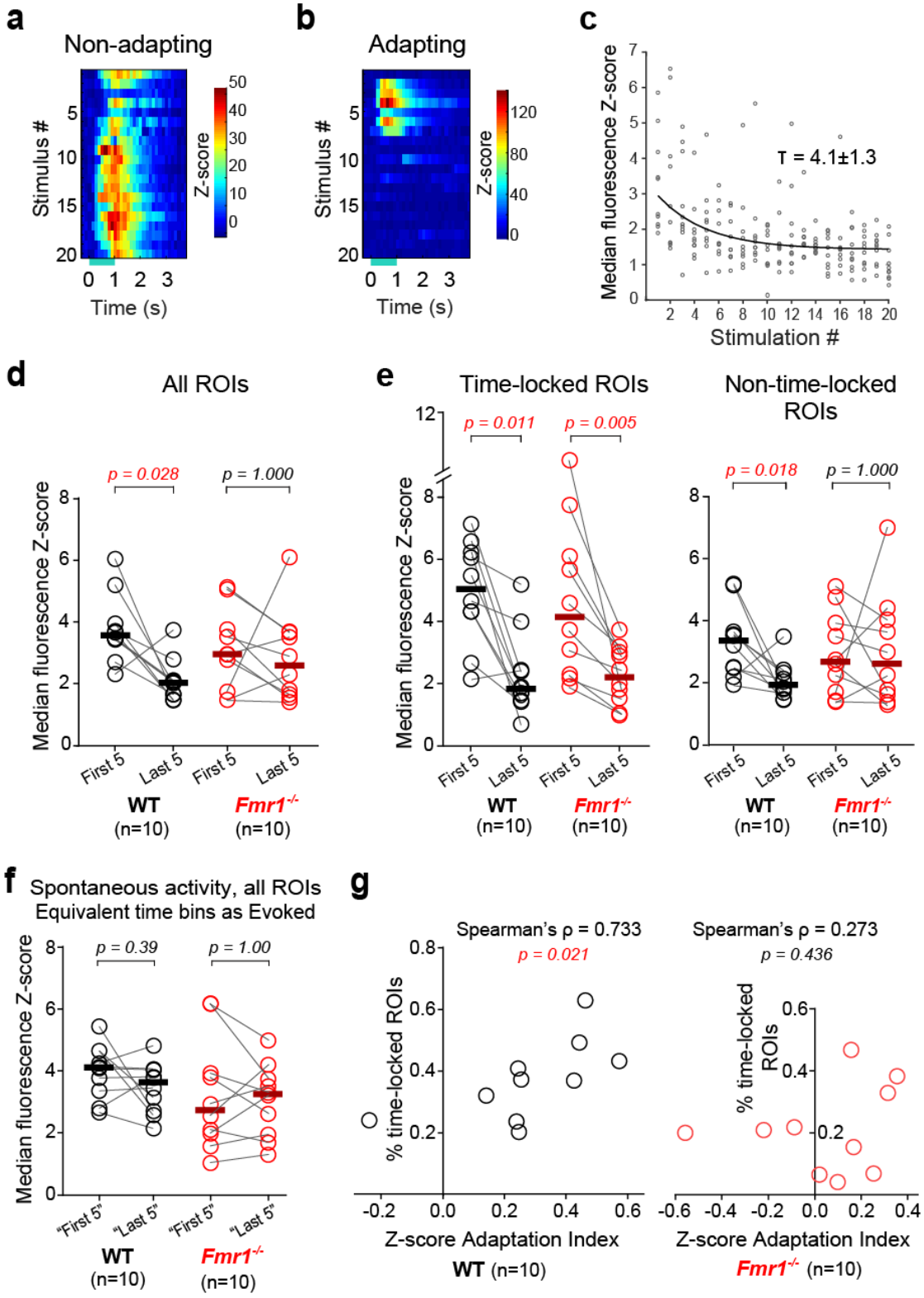

Fig. 9: Lack of adaptation of whisker-evoked activity in local networks of P14-16 *Fmr1*$^{-/-}$ mice

(a-b) Heatmaps of activity from example P14-16 WT L2/3 neurons showing adaptation (a) or no adaptation (b) during 20 consecutive whisker stimulations (y-axis). For panels (a-c), median fluorescence Z-scores per animal were binned from 0.2 s before stimulation onset to 2.8 s after stimulation end.

(c) Median Z-scores for P14-16 WT mice (n=10) during each stimulation bin, with exponential curve fit (see Methods).

(d) Median Z-scores of whisker evoked activity across all L2/3 neurons during the specified time bin during First 5 and Last 5 stimulations in WT and *Fmr1*$^{-/-}$ mice at age P14-16 (n=10 mice per genotype). For panels (d-f), the median fluorescence Z-scores per animal were binned from the start of the first stimulation to 3 s after the end of the fifth stimulation. Each circle represents a different animal. Bars represent group medians. P-values result from pairwise rank-based comparisons with 10,000 resamples and Bonferroni correction.

(e) Median Z-scores of whisker-evoked activity across time-locked and non-time-locked L2/3 neurons during First 5 and Last 5 stimulations in WT and *Fmr1*$^{-/-}$ mice at P14-16.

(f) Median Z-scores of spontaneous activity across all ROIs at P14-16, binned using the same start and end times as used to analyze whisker-evoked activity in (d-e).

(g) Percentages of time-locked ROIs in WT and *Fmr1*$^{-/-}$ mice at P14-16, plotted against Z-score Adaptation Indices, with Spearman's correlations. Adaptation Index = (Z-score during First 5 stimulations – Z-score during Last 5 stimulations) / (Z-score First 5 + Z-score Last 5). P-values from bootstrapping with 10,000 resamples.

Based on both the behavioral and imaging findings of defective adaptation in the P14-16 *Fmr1*$^{-/-}$ animals, we hypothesized that these defects would be linked, i.e., that a lack of adaptation in the activity of L2/3 neurons correlates with a persistence of locomotion during repetitive whisker stimulation. In an additional set of five P14-16 *Fmr1*$^{-/-}$ animals, we performed injections of GCaMP6s viral vector at P1, cranial window surgeries at P10-11, ball treadmill habituation for three consecutive days between P11-14, and behavioral testing and calcium imaging at different times within P14-16. To quantify the degree of network and behavioral adaptation we again calculated Adaptation Indices:

$$\frac{(X\ during\ First\ 5\ stimulations) - (X\ during\ Last\ 5\ stimulations)}{(X\ during\ First\ 5\ stimulations) + (X\ during\ Last\ 5\ stimulations)},$$

where X = Z-score of fluorescence or X = time with ball movement for each animal. The findings were inconclusive in this small sample size (**Fig. 10**), although 4 of the animals appear in the quadrants that suggest a relationship between the two measures.

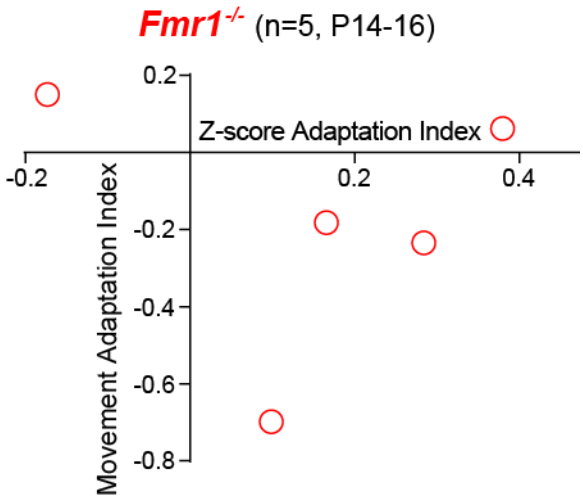

Figure 10: Neuronal and movement adaptation during repetitive whisker stimulation in the same animals

Movement adaptation in five WT and *Fmr1*$^{-/-}$ mice at P14-16, plotted against Z-score Adaptation Indices. Adaptation Index = (Z-score or time moving during First 5 stimulations – Z-score or time moving during Last 5 stimulations) / (Z-score First 5 + Z-score Last 5).

Impaired adaptation of local whisker-evoked neuronal activity in *Fmr1*$^{-/-}$ mice persists into adulthood

Finally, we tested whether a similar lack of neuronal sensory adaptation was evident in adult *Fmr1*$^{-/-}$ mice, given that they show a clear avoidance response to repetitive whisker stimulation. We injected the AAV vector for GCaMP6s expression at 2-4 weeks before imaging and confirmed barrel cortex targeting using optical intrinsic signal imaging (see **Methods**). We did not find significant differences between adult WT and *Fmr1*$^{-/-}$ mice (P34-74) in equivalent periods of spontaneous or whisker-evoked activity (p=1.00 by two-group comparison, **Fig. 11a**). In contrast to P14-16 mice, we did not find a difference in the proportion of time-locked L2/3 neurons between adult WT and *Fmr1*$^{-/-}$ mice (p=0.35 by two-group comparison, **Fig. 11b**). However, whereas adult WT mice exhibited robust neuronal adaptation to repetitive whisker stimulation (Z-scores: 2.42±0.53 first five vs. 1.58±0.53 last five, p=0.012 by two-group comparison, **Fig. 11c**), adult *Fmr1*$^{-/-}$ animals did not (2.18±0.34 first five vs. 2.20±0.50 last five, p=1.000, **Fig. 11c**).

In adult WT mice, both time-locked and non-time-locked cells showed adaptation (p=0.012 and p=0.066, **Fig. 11d**), but adult *Fmr1*$^{-/-}$ mice did not show adaptation in either subset of cells (p=0.258 and p=1.000, **Fig. 11d**). There was again no change in spontaneous activity of all ROIs between the equivalent "first five" and "last five" time bins (**Fig. 11e**). On the whole, the data in adult mice was similar to the results in P14-P16 mice. The lack of modulation of the activity of non-time-locked cells in *Fmr1*$^{-/-}$ mice (especially at P14-P16) appears to be responsible for the overall network adaptation defect observed during repetitive whisker stimulation.

Figure 11:
Lack of adaptation of whisker-evoked activity in local networks of adult *Fmr1*$^{-/-}$ mice

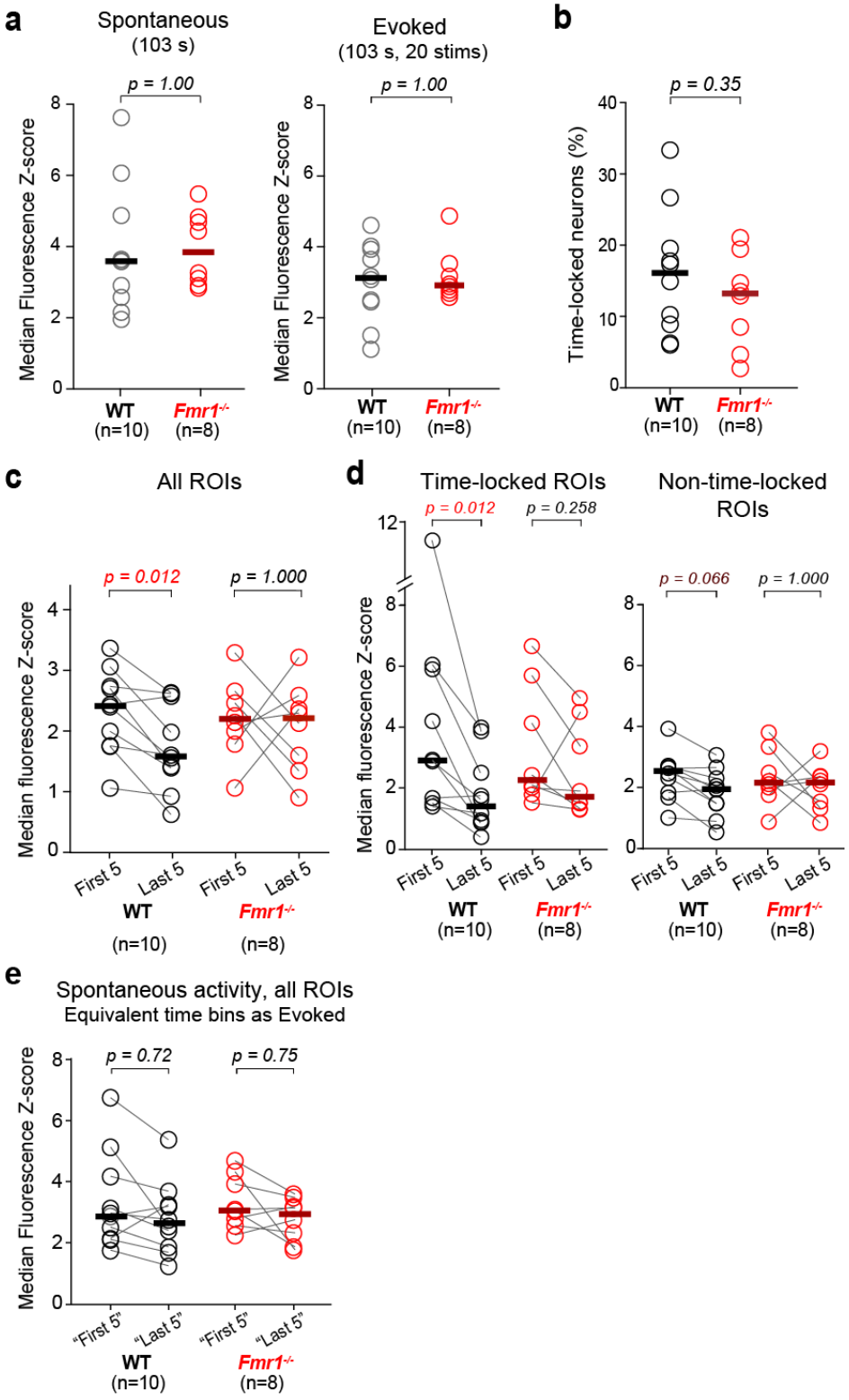

Fig. 11: Lack of adaptation of whisker-evoked activity in local networks of adult *Fmr1*$^{-/-}$ mice

(a) Median Z-scores for spontaneous (left) and whisker-evoked activity (right) of L2/3 neurons in WT and *Fmr1*$^{-/-}$ mice at P34-74 (n= 10 WT mice and n=8 *Fmr1*$^{-/-}$ mice). Each circle shows the median Z-score across all ROIs for one animal, for equivalent durations of spontaneous and evoked imaging (103 s). In (a-e), bars represent group medians and p-values were obtained from two-group rank-based comparisons with 10,000 resamples, with pairwise comparisons and Bonferroni correction for (c-e).

(b) The proportion of time-locked neurons is not different between WT and *Fmr1*$^{-/-}$ adult mice (n= 10 WT mice and n=8 *Fmr1*$^{-/-}$ mice). Each circle represents a different animal.

(c) Median Z-scores of whisker evoked activity across all L2/3 neurons during the specified time bin during First 5 and Last 5 stimulations in WT and *Fmr1*$^{-/-}$ mice at age P34-74. For panels (c-e), the median Z-scores per animal were binned from the start of the first stimulation to 3 s after the end of the fifth stimulation.

(d) Median Z-scores of whisker-evoked activity across time-locked and non-time-locked L2/3 neurons during First 5 and Last 5 stimulations at P34-74.

(e) Median Z-scores of spontaneous activity across ROIs at P34-74, binned using the same start and end times as used to analyze whisker-evoked activity in (c-d).

METHODS

Cranial window surgery for P14-16 imaging.

Full details are given at the end of Chapter 2. In brief, pups (P10-12) were anesthetized with isoflurane (5% induction, 1.5-2% maintenance via a nose cone, vol/vol) and placed in a stereotaxic frame. A 2.5-3.5 mm diameter craniotomy was performed over the right barrel cortex and covered with a 3 or 5 mm glass coverslip, as previously described (Mostany and Portera-Cailliau, 2008; Golshani et al., 2009). A headbar was also attached to the skull with dental cement to secure the animal to the microscope stage.

Cranial window surgery with AAV vector injection for adult GCaMP6s imaging

For 8 of the 10 WT adult animals and 5 of the 8 *Fmr1*$^{-/-}$ adult animals imaged, the AAV1.Syn.GCaMP6s.WPRE.SV40 vector was injected into the barrel cortex during the cranial window surgery, following existing protocols (Chen et al., 2013). After creation of a 4 mm craniotomy over the right barrel cortex, approximately 30 nL of rAAV vector, diluted to a working titer of 2e13 with 1% filtered Fast Green, was injected into 4-7 sites in the barrel cortex. The craniotomy was covered with a 5 mm glass coverslip, and a headbar was also attached to the skull with dental cement. For 2 of the 10 WT adult animals and 1 of the 8 *Fmr1*$^{-/-}$ adult animals, the rAAV vector had been injected at P1, following the previously described protocol, but was not

included in the P14-16 imaging experiments. The remaining 2 of 8 *Fmr1*$^{-/-}$ adult animals had been injected with rAAV vector at P1, and were also included in the P14-16 imaging experiments.

Optical Intrinsic Signal (OIS) imaging.

Following cranial window surgery, OIS imaging was used to map the barrel cortex at P12-14 (for P14-16 imaging) or at least 1 day before imaging (for adults). As previously described (Johnston et al., 2013), the contralateral whisker bundle was gently attached using bone wax to a glass needle coupled to a piezo-actuator (Physik Instrumente). Each stimulation trial consisted of a 100 Hz sawtooth stimulation lasting 1.5 s. The response signal divided by the averaged baseline signal, summed for all trials, was used to generate the cortical representation of stimulated whiskers (**Fig. 7b**).

***In vivo* two-photon calcium imaging in head-restrained mice.**

Calcium imaging was performed on a custom-built two-photon microscope, with a Chameleon Ultra II Ti:sapphire laser (Coherent), a 20X objective (0.95 NA, Olympus) and ScanImage software (Pologruto et al., 2003). Mice were lightly sedated with chlorprothixene (2 mg/kg, i.p.) and isoflurane (0-0.5%), and kept at 37°C using a temperature control device and heating blanket (Harvard Apparatus). The isoflurane was manually adjusted to maintain a breathing rate ranging from 100-150 breaths/min for P14-16 mice and 140-150 breaths/min for adult mice. Both

spontaneous activity and whisker-evoked barrel cortex activity were recorded. Whisker stimulation was delivered by bundling the contralateral whiskers (typically all macrovibrissae of at least ~1 cm in length), via soft bone wax, to a glass needle coupled to a piezo-actuator (**Fig. 7a** right). The stimulation protocol was the same as that used during behavioral experiments (**Fig. 7d**). Whole-field images were acquired at 7.8 Hz (1024 x 128 pixels downsampled to 256 x 128 pixels) (**Fig. 7c**).

Data analysis for calcium imaging.

Calcium imaging data were analyzed using custom-written MATLAB routines, which included modifications over previously described MATLAB code (Golshani et al., 2009; Gonçalves et al., 2013). In 4 out of 20 movies of P14-16 spontaneous activity (1,600 frames acquired), between 8 and 34 frames with significant Z-motion were manually removed before motion correction. In 1 out of 20 movies of P14-16 evoked activity (800 frames), 24 frames with Z-motion occurred during the initial 10 seconds of baseline acquisition before whisker stimulation began, allowing replacement of these frames with an averaged Z-projection of the remainder of the video. In 11 out of 20 movies of P34-74 spontaneous activity (1,600 frames acquired), some frames (up to 420) exhibiting Z-axis motion were manually removed before motion correction. Subsequent data quantifications used only the first 800 frames of spontaneous activity, i.e., an equivalent duration as the evoked activity.

X-Y drift in the movies was then corrected using either a frame-by-frame, Hidden-Markov-Model-based registration routine (Dombeck et al., 2007) or a cross-correlation-based, non-rigid alignment

algorithm (Mineault et al., 2016). A semi-automated algorithm (Chen et al., 2013) was used to select regions of interest, each representing a single cell body, and extract the fluorescence signal ($\Delta F/F$) for each neuron. A "modified Z-score" Z_F vector for each neuron was calculated as

$$Z_F = \frac{F(t) - mean(quietest\ period)}{std(quietest\ period)},$$

where the quietest period is the 10 s period with the lowest variation (standard deviation) in $\Delta F/F$. All subsequent analyses were performed using the Z_F vectors.

To define whether an individual cell showed time-locked responses to whisker stimulations, a probabilistic bootstrapping method was implemented. First, we calculated the correlation between the stimulus time-course and the Z_F vector, followed by correlation calculations between the stimulus time-course and 10,000 scrambles of all calcium activity epochs in Z_F (epoch = consecutive frames wherein Z_F $\geq$ 3). The 10,000 comparisons generated a distribution of correlations (R values), within which the correlation of the unscrambled data and the stimulus fell at a certain percentile. If the calculated percentile for a cell was less than 0.01, then we described that cell as being time-locked.

For analysis of aggregate activity within a particular time range, e.g. First 5 stimulations or 800 frames, the mean of Z_F within that time range was calculated for each ROI, and for each animal imaged, a median Z_F was then calculated across all ROIs or a subset of ROIs (e.g. only time-locked or non-time-locked ROIs). The initial and end baseline periods of Evoked activity were included in the analyses for **Figs. 7f, 7h,** and **11a-b**.

For curve fitting of WT neuronal activity across stimulations (**Fig. 9c**), we calculated the median Z_F across ROIs for each animal imaged, within each of the 20 stimulations (from 0.2 s before stimulation onset to 2.8 s after stimulation end), and then applied iterative nonlinear, least-squares curve fitting with the Levenberg-Marquardt algorithm. The best-fit exponential curve to all data points for each stimulation had the equation $y = Ae^{-x/\tau} + off$, where A = 1.94±0.25, τ = 4.10±1.26, and *off* = 1.42±0.14.

Chapter **4**

Discussion

Answers were important, the canyon said,
But the answers were not the solution.

--- from “Adolescence,” by Adrienne Su

Defects in neuronal and behavioral adaptation during tactile stimulation in *Fmr1*$^{-/-}$ mice

A common symptom in FXS is abnormal sensory reactivity, which frequently manifests as tactile defensiveness (Liss et al., 2006; Sinclair et al., 2016). Sensory overreactivity is significant because it can contribute to other symptoms, such as anxiety, sleep disturbances, seizures, and inattention, and ultimately disrupt daily living. Tactile hypersensitivity is also seen in other ASDs; indeed, one study of children with autism found that 60% (of 171) of children with autism showed tactile symptoms, particularly manifesting during grooming and hygiene activities (Tomchek and Dunn, 2007). Clinical interventions to improve sensory modulation in ASDs rely on behavioral or pharmacological treatments that are not specific for the underlying disorder (van Karnebeek et al., 2016). Coinciding with the disappointments of recent clinical trials aimed at molecular targets (Mullard, 2015), neuroscientists are increasingly turning to *in vivo* recordings of network activity in rodent models of ASDs (Gonçalves et al., 2013; Arnett et al., 2014; Zhang et al., 2014; Lu et al., 2016) to discover new therapeutic targets.

We followed such a symptom-to-circuit approach and designed our experiments to characterize circuit-level defects that underlie sensory overreactivity in the *Fmr1*$^{-/-}$ mouse model of FXS. We established a new behavioral assay for tactile defensiveness in both young and adult mice, and used *in vivo* calcium imaging with GCaMP6s to record ensemble activity of L2/3 neurons in the barrel cortex. Our main results were as follows: 1) P14-16 *Fmr1*$^{-/-}$ mice demonstrate an exaggerated locomotor response during repetitive whisker stimulations; 2) Adult *Fmr1*$^{-/-}$ mice show an avoidance response to repetitive whisker stimulation, resembling tactile defensiveness in FXS patients; 3) Unexpectedly, we found no evidence of exaggerated sensory-evoked neuronal activity in L2/3 of young or adult *Fmr1*$^{-/-}$ mice; 4) The proportion of L2/3 neurons in barrel cortex

that responds in a time-locked manner to whisker stimulation is 45% lower in *Fmr1*$^{-/-}$ mice compared to WT mice at P14-16; 5) Neuronal activity in *Fmr1*$^{-/-}$ mice at both P14-P16 and P34-74 shows a lack of adaptation to repetitive whisker stimulation. Our results indicate that the absence of adaptation within local neuronal networks is a likely contributor to sensory overreactivity in FXS, and perhaps in other ASDs.

Active avoidance of tactile stimulation is challenging to study during early postnatal ages because of the small size and limited locomotion of neonatal mouse pups. Although spontaneous whisker movements begin during the first postnatal week (Akhmetshina et al., 2016), mice do not show robust locomotion or true exploratory whisking before P13 (Arakawa and Erzurumlu, 2015; van der Bourg et al., 2016). Remarkably, our novel behavioral assay for head-restrained mice identified a behavioral equivalent of human tactile defensiveness: not only did we observe a pronounced increase in locomotion with repetitive whisker stimulation in P14-16 *Fmr1*$^{-/-}$ mice (which we interpret as an escape behavior), but there was also a clear avoidance response (turning away from the aversive stimulus) in adult *Fmr1*$^{-/-}$ mice.

Considering that FXS symptoms present in the first year of life, we chose to carry out experiments during the second postnatal week, a critical age in mice analogous to an early perinatal period when sensory experience shapes somatosensory cortex in humans (Workman et al., 2013). The second postnatal week coincides with the onset of robust active whisking and with the consolidation of anatomical and functional "barrel" maps in the mouse cortex (Petersen, 2007). Our results add to the notion that alterations in circuits during critical periods of experience-dependent plasticity are fundamental to the pathophysiology of FXS (Bureau et al., 2008; Cruz-

Martín et al., 2010; Harlow et al., 2010; Gonçalves et al., 2013; He et al., 2014) and ASDs in general (Meredith et al., 2012), even if they endure into adulthood.

For our behavioral and calcium imaging experiments we chose to stimulate groups of whiskers to better mimic the passive whole-snout inputs derived from long bouts of contact with littermates and from grooming by the dam, which dominate the animals' early somatosensory experience. Our stimulation frequency and timing were also physiologically relevant, as exploratory whisking in mice is typically 5-15 Hz in 1-4 s bouts (Kleinfeld et al., 2006). Whereas each of our 20 stimulations was relatively physiological in scale and magnitude (1 s at 10 Hz), the repetitive nature of the entire 80 s stimulation series was intentionally chosen to be more akin to a environmental stimulation that might be perceived as persistently irritating (e.g., wearing certain clothes), without being shocking (e.g., a brief but extremely loud sound). Our results on neuronal adaptation to repetitive whisker stimulation in early postnatal WT mice are consistent with those of a recent study of using multi-electrode array recordings (van der Bourg et al., 2016), in which barrel cortex activity in young mice was recorded during ten consecutive 10 ms-long whisker deflections (200 ms ISI). It is important to note that the time course of stimulation and adaptation we chose is particularly relevant to studying the problem of tactile defensiveness in autism.

In addition to running on the ball as a putative escape response to aversive stimulation, additional behaviors of interest include batting or grabbing at the stimulator, as well as pupil diameter as a measure of arousal (Reimer et al., 2014). We had examined durations of contact between the animals' paws and the stimulator by attaching the stimulator's wires to a capacitive touch sensor breakout board, but we did not observe differences between genotypes, nor was batting a consistent phenotype within either of the genotypes. In other experimental work, our group has observed

that stimulation frequencies above 50 Hz elicit much more frequent batting motions, and as such, the 10 Hz stimulation frequency was probably not aversive enough to make this behavior a useful metric in this study. We also attempted to measure pupil diameters using an additional camera inside the behavior rig, but found that the P14-16 mice do not keep their eyelids open wide enough to permit constant visualization of the pupil. Our rig interior lighting was also too dim to maintain the adult animals' pupils at a sufficiently small baseline diameter to measure fluctuations during the sensory stimulation.

In adult mice, brief (200 ms) deflections of 2-3 whiskers cause inter-whisker inhibition between barrel cortex neurons within <500 ms (Simons, 1985); conversely, during 10 Hz multi-whisker stimulations lasting 1 s, adaptation of barrel cortex neurons enables "surround facilitation" instead of suppression (Ramirez et al., 2014). As we examined neuronal adaptation over much longer time scales, it is unlikely that single-whisker stimulation would reveal different results (in other experiments, we find that single-whisker stimulation also leads to neuronal adaptation in WT mice; data not shown). One caveat regarding the interpretation of our results is that we imaged L2/3 activity in barrel cortex of mice that were lightly sedated, in order to maintain a consistent behavioral state, as well as to minimize active whisking events that might contribute to feedback-enhanced cortical activity and contaminate our recordings (Petersen, 2007). While deep anesthesia via >1% isoflurane is known to produce a markedly different neuronal activity pattern from the awake state, the use of light (<0.5%) isoflurane has been shown to allow a sparse, desynchronized pattern of neuronal population activity that is similar to the awake state (Lissek et al., 2016).

In our experiments of imaging and behavior in the same five P14-16 animals, we were unable to demonstrate a correlation between the degree of neuronal adaptation and the degree of locomotor

adaptation during repeated whisker stimulation. This certainly does not mean that the two defects are in fact linked, as we still believe them to be, but that a small sample size is insufficient to demonstrate the presence or lack of such an association. We had attempted to perform simultaneous imaging and behavior assessment with the animals fully awake and non-sedated on the running ball treadmill. However, we found that even after three days of ball habituation and use of a new headbar design with two-point fixation, locomotion of the young pups caused too much motion in the Z direction to allow for stable visualization of the same ROIs. We suspect that this is due to the softness of the skull and openness of sutures during the earliest weeks of life. As such, we had to perform the behavioral testing and imaging at different times, greatly reducing our ability to link the imaging and behavioral phenotypes.

It was not surprising that the degree of L2/3 neuronal adaptation correlated well with the proportion of L2/3 neurons showing time-locked responses to whisker stimulations in the WT mice, but not in the *Fmr1*$^{-/-}$ mice. It may be intuitive that a critical number of neurons within a local network must respond robustly to a particular stimulation pattern in order for those neurons, and for the neurons to which they connect, to adapt. Accordingly, we observed that both the time-locked and non-time-locked neuronal subpopulations in the WT showed adaptation over the course of 20 stimulations. However, if the *Fmr1*$^{-/-}$ mice lack enough spatial density of time-locked L2/3 neurons to drive overall adaptation across the local networks, that could explain our observation that the time-locked neurons did show adaptation in the *Fmr1*$^{-/-}$, but the non-time-locked subpopulations did not.

An unexpected finding of our study was that the proportion of time-locked L2/3 neurons was much lower in *Fmr1*$^{-/-}$ than in WT animals at P14-16 (though not evident in adult mice), and that sensory

stimulation did not trigger abnormally high activity in neurons from *Fmr1*$^{-/-}$ mice at either age. These results seem to contradict predictions of the theory of neuronal and network hyperexcitability in FXS (Contractor et al., 2015). However, the L2/3 activity from a single whisker stimulation is known to be distributed across several cortical columns (Clancy et al., 2015). It is possible that in *Fmr1*$^{-/-}$ mice the functional circuits for whisker touch processing are dispersed over an even larger spatial area, resulting in an apparently reduced proportion of time-locked neurons within any given local network (about 200 μm in diameter), as we observed. Indeed, recent studies using OIS and *in vivo* electrophysiology found that stimulation of a single whisker resulted in a larger spatial area of activation across the *Fmr1*$^{-/-}$ barrel cortex, compared with WT (Arnett et al., 2014; Juczewski et al., 2016).

Potential mechanisms underlying neuronal adaptation defects in the *Fmr1*$^{-/-}$

Our results prompt speculation regarding how connectivity within local networks differs between the WT and *Fmr1*$^{-/-}$ barrel cortices or other cortical areas. It is possible that there are genotype-specific differences in the prevalence or function of so-called "hub neurons," which are cells with high functional connectivity and high impact on local network dynamics (Cossart, 2014). Hub neurons have been characterized as GABAergic cells, crucial for synchronizing hippocampal network oscillations (Bonifazi et al., 2009), but have been less frequently studied in the cortex (Shimono and Beggs, 2015). If adaptation of hub neurons was in fact necessary to drive the entire network's adaptation, and if the *Fmr1*$^{-/-}$ cortex had fewer such hub neurons, then the resulting

activity patterns would in fact be more poorly organized, with a broader spatial distribution (as others have published) and with reduced adaptation, as we observed.

The ideas of hub neurons and hyperexcitability also call into question the roles of interneurons in *Fmr1*$^{-/-}$ circuit dysfunction. Earlier work has found a decrease in inhibitory interneuron drive, delayed GABA polarity switch, and a reduced density of PV interneurons in the *Fmr1*$^{-/-}$ somatosensory cortex (Selby et al., 2007; He et al., 2014; Tyzio et al., 2014; Lovelace et al., 2016). We used a recently described *post hoc* kurtosis filter (Ringach et al., 2016) to try and isolate the putative interneurons in our GCaMP6 imaging. However, we did not find differences in adaptation profile between the high-kurtosis (excitatory) and low-kurtosis (mixed excitatory and inhibitory) neurons. This kurtosis filter's utility was limited in our data because 1) this filter isolated one relatively homogenous population of pyramidal neurons from one heterogeneous population, with the latter comprising over 50% of our imaged neurons; and 2) our data sets were too small, i.e. well under 100 neurons per local network. Ongoing experiments in our lab are using imaging and electrophysiology of fluorescently labeled interneuron populations to specifically characterize the role of interneurons in primary visual cortex activity and visual perceptual deficits of the *Fmr1*$^{-/-}$ mice. The lab will eventually seek to do so in the barrel cortex as well.

Adaptation of cortical neurons to repeated or ongoing sensory stimulation is a robust phenomenon across sensory modalities (Ohzawa et al., 1982; Castro-Alamancos, 2004; Khatri et al., 2004; Ulanovsky et al., 2004), enabling increased detection, discriminability, and gain control (Castro-Alamancos, 2004; Ollerenshaw et al., 2014). The thalamocortical synapse is the principal site of cortical adaptation to repeated whisker stimulations, with additional adaptation occurring within L2/3 and L4 (Chung et al., 2002; Khatri et al., 2004; Heiss et al., 2008). Previous studies in the

Fmr1$^{-/-}$ somatosensory cortex have identified specific functional defects in thalamocortical synapses during both development (Harlow et al., 2010) and adulthood (Gibson et al., 2008); as well as defects in transmission and experience-dependent plasticity in L4-to-L3 projections (Bureau et al., 2008). The neuronal adaptation defect we observed in L2/3 cortical neurons of *Fmr1*$^{-/-}$ could also reflect upstream changes in sensory neurons in the periphery, brainstem, thalamus, or even in L4 neurons of barrel cortex. For example, a recent study identified hyperexcitability in peripheral somatosensory neurons of several mouse models of ASDs (Orefice et al., 2016), and the same defects could be present in *Fmr1*$^{-/-}$ mice. More work is needed to establish whether a loss of adaptation originates in the periphery and then spreads to somatosensory cortex, or whether it occurs simultaneously throughout the brain.

Our findings raise additional questions about the role of downstream brain regions in translating a lack of neuronal adaptation in somatosensory cortex into an avoidance/escape response to an aversive sensory stimulus. Altered sensory adaptation in *Fmr1*$^{-/-}$ circuits could also involve infragranular output layers (L5/6) in barrel cortex. However, in early postnatal normal mice, L5 and L6 neurons tend to show facilitation (i.e., an increase in activity, not a decrease) to repetitive whisker stimulation (van der Bourg et al., 2016), making an adaptation defect less likely at this step of the pathway. Beyond the cortex, the amygdala is almost certainly involved in autistic overreactivity to sensory stimuli (Green et al., 2015), and outputs of the basal ganglia were recently shown to modulate active avoidance (Hormigo et al., 2016). Future studies will need to address how specific brain regions (e.g., amygdala, periaqueductal gray, or cingulate), pathways, and neurotransmitters are involved in top-down modulation of tactile defensiveness, and we have shown that *Fmr1*$^{-/-}$ mice are an ideal model in which to study these questions. One hypothesis is that neuronal activity in the amygdala is necessary to translate an incoming sensory stimulation

into a perception of aversion or annoyance, resulting in a locomotor escape response. Experiments recently underway in the lab include the infusion of muscimol into the amygdalas of *Fmr1*$^{-/-}$ pups to potentially modulate their behavioral response to repetitive whisker stimulation.

Future directions

Given our findings, *Fmr1*$^{-/-}$ mice would be expected to show impairments in behavioral tasks that assess tactile perception and perceptual decision-making. Indeed, unpublished work from our lab has found that *Fmr1*$^{-/-}$ mice are slower to learn a visual discrimination task, and also show reduced performance with increased task difficulty or with distractors. In the somatosensory modality, published studies of the adult *Fmr1*$^{-/-}$ mouse have reported functional deficits in whisker sampling, gap-crossing, and texture discrimination (Arnett et al., 2014; Juczewski et al., 2016; Orefice et al., 2016), but these deficits have not been demonstrated in younger animals during critical periods of sensory plasticity. Our present results have demonstrated the feasibility of a head-fixed behavioral setup for testing reactions to passive sensory stimulation in early postnatal mice. Assessing perceptual decision-making in young pups is certainly of interest, but is more technically difficult because a week of consecutive training days may be necessary before testing on head-fixed or navigational tasks, because these tasks frequently require sensorimotor maturity, and because adult animals frequently need to be motivated by food or water restriction (Arnett et al., 2014; Guo et al., 2014), which would be dangerous in pups.

However, it is also possible to assay whisker-based texture discrimination in adult mice using a modified novel object recognition task, with only three days of brief (10 min) training sessions,

and without food or water restriction (Wu et al., 2013). During the first two postnatal weeks, pups are highly motivated by warmth (huddling with littermates) as well as feeding. Perhaps a task similar to the one described by Wu et al., involving association between a warm (preferred) location and a particular surface texture, with a sweetened milk reward, could be implemented with P14-16 pups. During several days of habituation, beginning soon after the onset of exploratory locomotion at P10-11, pups could be repeatedly placed in a small (cage-sized) square arena, in which each of the four corners has a different floor and wall texture. The relative positions of the four textures would be randomized across training trials, but one texture would consistently be linked to warming of that corner by a heating pad, as well as the milk reward when the pup reaches that corner and stays there for a certain amount of time. On the testing day, the pup could be placed in the same type of arena, but without any heated corner. The pup should seek out the texture that was associated with warmth, and I hypothesize that the *Fmr1*$^{-/-}$ pups would be less successful on this task, demonstrating a texture discrimination deficit and/or a somatosensory learning deficit; I also hypothesize that task performance would be correlated with other measures of behavioral tactile dysfunction and abnormal cortical response. Such a task would assay deficits in both whisker-based and skin-based somatosensory processing; the latter is also of interest, given the recent finding of peripheral somatosensory neuronal hyperexcitability in other adult mouse models of ASD (Orefice et al., 2016).

It is also interesting to consider how altered somatosensory adaptation (as we have shown) and reduced sensory discrimination and decision-making (as in the published gap-crossing deficits) might be more directly linked in the *Fmr1*$^{-/-}$ mouse. One study using voltage-sensitive dye imaging in WT adult rats showed that delivery of a 1 s 10 Hz "adapting stimulus" to a single whisker caused spatial reduction of the cortical response to subsequent deflection of that whisker, as well as

increased separation of the cortical response maps for that whisker and an adjacent whisker, i.e., improved cortical discriminability (Ollerenshaw et al., 2014). The same study also used a head-fixed whisker discrimination task wherein rats had to detect stimulation of one whisker or an adjacent whisker, with the test stimulus preceded by the same 1 s "adapting stimulus" in 50% of the trials (Ollerenshaw et al., 2014). During the condition with adapting stimulus, stimulus detectability decreased, but whisker discrimination performance – behavioral discriminability – improved (Ollerenshaw et al., 2014). This study was performed in rats and required a long habituation and training period, but the adapting stimulus had the same length and frequency as a single stimulation from our 20-stimulation series, making Ollerenshaw et al.'s findings even more relevant to our present paradigm. We showed that the L2/3 neuronal adaptation defect in *Fmr1*$^{-/-}$ mice persists into adulthood, and prior findings of larger receptive fields in the *Fmr1*$^{-/-}$ barrel cortex suggest decreased baseline cortical discriminability for whisker inputs. If the adaptation defect is present at both short (1 s) and long time scales (as we used), then the animals' perceptual threshold might remain low (detectability remaining high) after stimulus exposure has begun, instead of decreasing appropriately, which could contribute to the behavioral defensiveness. At the same time, due to the adaptation defect, the *Fmr1*$^{-/-}$ animals' cortical and behavioral discriminability might remain too poor to allow successful learning or performance on a whisker discrimination task. These hypotheses are certainly worth testing in the *Fmr1*$^{-/-}$ model, especially since cognitive deficits in this mouse model could have implications for our understanding of learning difficulties in children with FXS.

We believe that sensory processing and integration abnormalities contribute to not just cognitive deficits in ASDs, but also to repetitive behaviors and social behavior deficits. This interplay was certainly reflected in recent fMRI findings that adolescents with ASD show more effortful social

information processing – increased activity in frontotemporal language areas and prefrontal cortex – during the presence of a tactile sensory distractor (Green et al., 2017). It is necessary to test the link between sensory and social symptoms in animal models in order to demonstrate the role of sensory dysfunction as a core neurodevelopmental deficit in ASD. Of note, in the *Shank3B*$^{-/-}$ mouse model of autism, the most prominent behavioral phenotypes are reduced social interaction and dramatically repetitive grooming behaviors beginning in early adulthood (Peça et al., 2011), but these animals also have heightened whisker sensitivity and hyperactivity in the primary somatosensory cortex (Feng, 2016). The *Fmr1*$^{-/-}$ mouse also has a phenotype of tactile hypersensitivity (and defective tactile adaptation), as well as social interaction deficits and repetitive behaviors (Spencer et al., 2011), though the latter two deficits are less severe than in the *Shank3B*$^{-/-}$ model. I would hypothesize that in both of these animal models, the degree of behavioral and cortical tactile dysfunction would correlate with the severity of altered social behavior even before weaning age, and might also correlate with the onset or severity of repetitive grooming in the *Shank3B*$^{-/-}$ mice.

Another open question in the field of FXS research is the necessity of *Fmr1* expression and FMRP during prenatal and postnatal critical periods. Other mouse models of monogenic neurodevelopmental disease have been used to show the apparent sufficiency of gene expression in adulthood for restoration of a WT phenotype, or the necessity of specific gene expression during adulthood for maintenance of normal phenotype. Earlier work has used a conditional *Mecp2* knock-in model of Rett Syndrome, wherein the *Mecp2*$^{\text{lox-Stop}}$ allele was controlled by a *cre-ER* transgene (Guy et al., 2007). The mice carrying *Mecp2*$^{lox\text{-}Stop/y}$*,cre-ER* developed as *Mecp2* null mice, but the restoration of MeCP2 in adulthood via tamoxifen administration resulted in rescue of neurological phenotype and hippocampal LTP to levels comparable to the WT, even after the

emergence of disease symptoms (Guy et al., 2007). In a complementary study, mice carrying a floxed *Mecp2* and inducible Cre-ER were used to remove MeCP2 during adulthood, resulting in neurological and motor impairments comparable to *Mecp2* null animals (McGraw et al., 2011). More recently, the conditional *Shank3* knock-in mouse model was used to demonstrate that restoration of *Shank3* in adulthood rescued deficits in post-synaptic density protein expression, striatal neurotransmission, repetitive grooming, and social interaction; but not the deficits in anxiety, locomotion, motor coordination (Mei et al., 2016). It remains unknown whether the circuit and behavioral deficits caused by a lack of *Fmr1*/FMRP during prenatal and early postnatal development could be compensated for by later restoring *Fmr1* expression. A conditional *Fmr1*$^{-/-}$ mouse is available (Mientjes et al., 2006) and could be crossed with an inducible Cre-ER line to yield animals in which *Fmr1* expression is silenced at a specific developmental age and/or in a specific cell population. A conditional *Fmr1* knock-in mouse may still be under development (Mientjes et al., 2006). As was seen in the *Shank3* adult rescue experiments, it is very likely that adult restoration of *Fmr1* expression might restore some deficits, but not others; alternatively, restoration before the second postnatal week may be necessary in order to ensure normal circuit activity and sensory processing phenotypes. It is also possible that removal of *Fmr1* expression only during adulthood might not result in the same deficits that are seen in the *Fmr1*$^{-/-}$, because the circuits mediating sensory reactivity and sensory-based decision-making have already been consolidated during the early weeks of life.

The ultimate goal of studies that investigate abnormalities in network activity in *Fmr1*$^{-/-}$ mice is to identify effective treatments for the devastating symptoms of FXS. Beyond the mGluR or GABA theories of FXS, a growing body of work indicates that dysregulated signaling of the excitatory neurotransmitter acetylcholine (ACh) plays a significant role in FXS pathophysiology. ACh can

modulate cognition, arousal, and excitability, and is crucial for the response of neuronal ensembles to sensory input (Picciotto et al., 2012). An *in vitro* study found that the cholinergic agonist carbachol caused aberrantly increased excitatory responses in *Fmr1*$^{-/-}$ mice, providing early evidence that cholinergic signaling is enhanced in the KO (D'Antuono et al., 2003). Others have shown that the *Fmr1*$^{-/-}$ mice mouse has excessive muscarinic ACh receptor (mAChR) signaling causing abnormal long-term depression (Volk et al., 2007). Also interestingly, our lab previously found that the circuit hyperexcitability in the *Fmr1*$^{-/-}$ mice is heightened during times of sleep or rest (Gonçalves et al., 2013). Since an animal's state of vigilance is already known to be highly dependent on cholinergic tone (Lee and Dan, 2012), this further suggests that abnormal cholinergic tone may be responsible for circuit pathology in FXS.

Accordingly, future experiments should test the hypothesis that an excess of cholinergic tone could account for the observed defects in neocortical circuit and behavioral adaptation of *Fmr1*$^{-/-}$ mice. It would first be useful to investigate whether a mouse model already known to have increased ACh signaling could recapitulate the circuit defects seen in the *Fmr1*$^{-/-}$ mouse. Thus, *in vivo* imaging could be used to profile activity of L2/3 neurons in the barrel cortex of the *ChAT-ChR2-EYFP* mouse, which is a BAC transgenic model that overexpresses channel-rhodopsin 2 under the choline acetyl transferase promoter and was originally developed to enable optogenetic investigation of ACh neurotransmission (Zhao et al., 2011). However, because the vesicular ACh transporter gene (*VAChT*) lies within the *ChAT* gene, the BAC expressing *ChAT* also carries intact *VAChT*. This results in overexpression of the ACh transporter and a threefold increase in ACh release (Kolisnyk et al., 2013). Consistent with a pathological level of ACh signaling, these mice show increased physical endurance and deficits in motor learning, spatial and working memory, and attentional processing (Kolisnyk et al., 2013). Thus, even without optogenetic manipulations,

this mouse is an intrinsically useful model for studying the effects of excessive cholinergic tone. One could hypothesize that these mice also exhibit cortical network adaptation defects under repeated sensory stimulation, at both P14-16 and early adulthood. Examining spontaneous and evoked activity of L2/3 neurons in barrel cortex in this mouse model could provide a useful assessment of whether increased cholinergic tone can result in the same network abnormalities seen in the *Fmr1*$^{-/-}$ mice.

Since recent studies have shown that administration of an M1 or M4 mAChR antagonist can reduce behavioral defects in the *Fmr1*$^{-/-}$ (Veeraragavan et al., 2011a, 2011b), manipulation of cholinergic signaling may be a novel therapeutic strategy in FXS. While mAChR subtypes are complex and can be differentially antagonized by specific pharmacological agents, the effects of an anticholinergic drug on cortical network activity are unknown. The nonselective muscarinic antagonist scopolamine is a reasonable candidate for acute and chronic administration in *Fmr1*$^{-/-}$ mice (Constantinople and Bruno, 2011). Administration of this drug could potentially "normalize" the aberrant network activity by restoring a degree of adaptation during repetitive sensory stimulation, and might even reduce the associated behavioral defect.

***

We have concluded that altered sensory processing in the cortex might lead to anxiety and hyperarousal and ultimately contribute to the observed defensiveness behavior in *Fmr1*$^{-/-}$ mice. Our data fit well with not just the known behavioral phenotypes of *Fmr1*$^{-/-}$ mice and FXS patients, but also with existing EEG studies on sensory adaptation defects in *Fmr1*$^{-/-}$ mice and humans (Castren et al., 2003; Van der Molen et al., 2012; Ethridge et al., 2016; Lovelace et al., 2016;

Sinclair et al., 2016). A recent fMRI study also found a defect in adaptation to repeated tactile stimulus in the somatosensory cortex of patients (age 9-17) with both ASD and documented sensory overreactivity behavior (Green et al., 2015).

Our work encourages additional investigations using animal models of ASD at developmental stages to elucidate neuronal defects underlying aberrant behaviors that are relevant to human symptoms and function. The overarching goal is to connect specific genetic and molecular changes with specific circuit-level phenotypes and behavioral changes, as well as treatments targeted to those circuit and behavioral changes. Eventually, the management of ASD could begin with genetic diagnosis during routine prenatal or early postnatal screening, followed by neurological assessment using improved EEG and fMRI biomarkers during the first months and years of life. This neurodevelopmental monitoring could be used to design early behavioral support to improve the development of sensory integration, social communication, and other skills, before dysfunctions would normally become apparent and then impairing. Along with behavioral interventions to change the course of symptom development, targeted pharmacological treatments could be used to modulate circuit activity during these critical periods when these circuits, and their output behaviors, are being consolidated.

Appendix

Statistical approach

Based on my group sizes of n=8-10 for imaging data comparisons and n=13-21 for behavioral data comparisons, normality cannot be ensured, and tests of normality and variance are also unreliable. There is no consensus on a sample size threshold at which normality and variance testing becomes useful, potentially enabling parametric tests, though n>30 is frequently recommended and n>10 has been considered an "absolute minimum" (Corder and Foreman, 2009; Sullivan et al., 2016).

As such, I implemented a conservative statistical approach. Central tendencies are reported in the main text as group median with median absolute deviation. Graphs show all data points as well as group medians and, where error bars are shown, interquartile ranges. All statistical tests were rank-based comparisons with bootstrapping (10,000 resamples), without assumptions regarding normality or variance. These comparisons were implemented using custom-written R code. Paired rank-based comparisons were used when comparing measurements within the same animals (e.g. median fluorescence Z-scores during the first five vs. last five stimulations in WT mice). Unpaired rank-based comparisons were used when comparing measurements in different animals (e.g. % time-locked neurons in WT vs. *Fmr1*$^{-/-}$ mice). Two-sided p-values were calculated for each comparison, and Bonferroni corrections for multiple comparisons were applied where appropriate. The threshold for significance was set at $p<0.05$.

No statistical test was used to prospectively calculate sample sizes before experiments began. Target sample sizes were based on previous work from our group (Golshani et al., 2009; Gonçalves et al., 2013), and equal or exceed sample sizes for other recent studies using *in vivo* calcium imaging and head-fixed behavior. Certainly a single prospective calculation of power at the start of project design would have been ideal from both a statistical and ethical perspective, since sample sizes should be carefully chosen in order to use as few animals as possible. However, in our

experiments, the expected effect sizes are not known or easily estimated *a priori*, and a calculation of prospective power estimates for a range of effect sizes would result in a large range of potential sample sizes that would not aid in planning (or minimizing) animal usage.

Even smaller sample sizes than ours (e.g., n=5 animals) remain common in neuroscience, and it is also common in *in vivo* imaging studies to pool neurons from multiple animals and use a sample size of n = # of neurons imaged. However, I feel strongly that all neurons imaged within a single animal should be considered related, and thus integrated into a single data point whenever possible, as a number of variables differ uncontrollably between animals and imaging sessions (neurodevelopmental maturity of the individual mouse, its response to sedation or handling, whether the imaging area is more or less affected by the presence of blood vessels, the number of detectable ROIs, etc). Looking at my data, it is indeed clear that within the same genotype, animals vary greatly in their presentation of any imaging or behavioral phenotype.

It is well established that most neuroscientific studies are dramatically underpowered and thus suffer from both low positive predictive value and effect inflation (the so-called "winner's curse"). Button et al. examined a large cohort of published primary research studies and meta-analyses and reported, in 2013, that across neuroscience fields the median statistical power was 21%, or 18% if outliers are excluded (Button et al., 2013). For behavioral studies using animal models, they reported a median statistical power as 18% for medium effects and 31% for large effects (Button et al., 2013). With such low power, p-values also lose their meaning, and the reproducibility of results becomes much more difficult (Button et al., 2013; Krzywinski and Altman, 2013; Halsey et al., 2015).

My data are undoubtedly affected by these realities, and the apparent plague of underpowered studies in this field (including my own work) is disconcerting. However, Button et al. also acknowledge the "ongoing debate regarding the appropriate balance to strike between using as few animals as possible in experiments and the need to obtain robust, reliable findings" (Button et al., 2013). One power analysis I performed relatively early in my project suggested that sample sizes over 50 would be needed to achieve 80% power with α=0.05, but such large numbers of animal (per genotype) are unfeasible and arguably unconscionable. The actual number of animals used is always, in fact, much higher than the reported sample size, because of an unavoidable attrition of animals over the course of an experimental series: multiple intensive surgical and imaging procedures are involved, with unforeseen events such as cranial window not being clear enough for high-quality imaging, or viral vector expression not localized in the necessary area.

There is no clear solution to the problem of reasonable and feasible sample sizes being underpowered in biology. My approach has been to comprehensively report the data and openly acknowledge the limitations of our work, which include its limited sample sizes and low statistical power. Conclusions regarding circuit activity and behavior in mouse models of disease must ultimately rely on a range of studies from multiple labs, including ours, each providing some limited insight and incremental corroboration.

References

Akhmetshina D, Nasretdinov A, Zakharov A, Valeeva G, Khazipov R (2016) The Nature of the Sensory Input to the Neonatal Rat Barrel Cortex. J Neurosci 36:9922–9932.

American Psychiatric Assocation (2013) Diagnostic and statistical manual of mental disorders, 5th ed. Arlington, VA.

Arakawa H, Erzurumlu RS (2015) Role of whiskers in sensorimotor development of C57BL/6 mice. Behav Brain Res 287:146–155.

Arnett MT, Herman DH, McGee AW (2014) Deficits in Tactile Learning in a Mouse Model of Fragile X Syndrome. PLoS One 9:e109116.

Asperger H (1944) Die ,,Autistisehen Psychopathen" im Kindesalter. Arch Psychiatr Nervenkr 117:76–136.

Bailey A, Bolton P, Butler L, Couteur A Le, Murphy M, Scott S, Webb T, Rutter M (1993) Prevalence of the Fragile X amongst Autistic Twins and Singletons. :673–688.

Bakker CE, Verheij V, Willemsen R, van der Helm R, Oerlemans F, Vermey M, Bygrave A, Hoogeveen AT, Oostra BA, Reyniers E, De Boule K, D'Hooge R, Cras P, van Velzen D, Nagels G, Martin J-J, De Deyn PP, Darby JK, Willems, Patrick J Peter P. De Deyn, John K. Darby PJW (1994) Fmr1 Knockout Mice: A Model to Study Fragile X Mental Retardation. Cell 78:23–33.

Baranek GT, Roberts JE, David FJ, Sideris J, Mirrett PL, Hatton DD, Bailey, Jr. DB (2008) Developmental Trajectories and Correlates of Sensory Processing in Young Boys with Fragile X Syndrome. Phys Occup Ther Pediatr 28:79–98.

Belmonte MK, Allen G, Beckel-Mitchener A, Boulanger LM, Carper RA, Webb SJ (2004) Autism and Abnormal Development of Brain Connectivity. J Neurosci 24:9228–9231.

Ben-Ari Y (2015) Is birth a critical period in the pathogenesis of autism spectrum disorders? Nat

Rev Neurosci 16:498–505.

Ben-Sasson A, Cermak SA, Orsmond GI, Tager-Flusberg H, Carter AS, Kadlec MB (2007) Extreme sensory modulation behaviours in toddlers with autism spectrum disorder. Am J Occup Ther 61:584–592.

Bernardet M, Crusio WE (2006) Fmr1 KO mice as a possible model of autistic features. Sci World J 6:1164–1176.

Berry-Kravis EM, Hessl D, Rathmell B, Zarevics P, Cherubini M, Walton-Bowen K, Mu Y, Nguyen D V, Gonzalez-Heydrich J, Wang PP, Carpenter RL, Bear MF, Hagerman RJ (2012) Effects of STX209 (arbaclofen) on neurobehavioral function in children and adults with fragile X syndrome: a randomized, controlled, phase 2 trial. Sci Transl Med 4:152ra127.

Bonifazi P, Goldin M, Picardo M a, Jorquera I, Cattani a, Bianconi G, Represa a, Ben-Ari Y, Cossart R (2009) GABAergic hub neurons orchestrate synchrony in developing hippocampal networks. Science 326:1419–1424.

Brain KL, Bennett MR (1997) Calcium in sympathetic varicosities of mouse vas deferens during facilitation, augmentation and autoinhibition. J Physiol 502:521–536.

Brouwer JR, Mientjes EJ, Bakker CE, Nieuwenhuizen IM, Severijnen LA, Van der Linde HC, Nelson DL, Oostra BA, Willemsen R (2007) Elevated Fmr1 mRNA levels and reduced protein expression in a mouse model with an unmethylated Fragile X full mutation. Exp Cell Res 313:244–253.

Bureau I, Shepherd GMG, Svoboda K (2008) Circuit and plasticity defects in the developing somatosensory cortex of FMR1 knock-out mice. J Neurosci 28:5178–5188.

Butler MG, Mangrum T, Gupta R, Singh DN (1991) A 15-item checklist for screening mentally

retarded males for the fragile X syndrome. Clin Genet 39:347–354.

Button KS, Ioannidis JP a, Mokrysz C, Nosek B a, Flint J, Robinson ESJ, Munafò MR (2013) Power failure: why small sample size undermines the reliability of neuroscience. Nat Rev Neurosci 14:365–376.

Castren M, Paakkonen A, Tarkka IM, Ryynanen M, Partanen J (2003) Augmentation of auditory N1 in children with fragile X syndrome. Brain Topogr 15:165–171.

Castro-Alamancos MA (2004) Absence of Rapid Sensory Adaptation in Neocortex during Information Processing States. Neuron 41:455–464.

Chen Q, Cichon J, Wang W, Qiu L, Lee S-JR, Campbell NR, Destefino N, Goard MJ, Fu Z, Yasuda R, Looger LL, Arenkiel BR, Gan W-B, Feng G (2012) Imaging neural activity using Thy1-GCaMP transgenic mice. Neuron 76:297–308.

Chen T-W, Wardill TJ, Sun Y, Pulver SR, Renninger SL, Baohan A, Schreiter ER, Kerr R a, Orger MB, Jayaraman V, Looger LL, Svoboda K, Kim DS (2013) Ultrasensitive fluorescent proteins for imaging neuronal activity. Nature 499:295–300.

Christensen DL, Baio J, Braun KVN, Bilder D, Charles J, Constantino JN, Daniels J, Durkin MS, Fitzgerald RT, Kurzius-Spencer M, Lee L-C, Pettygrove S, Robinson C, Schulz E, Wells C, Wingate MS, Zahorodny W, Yeargin-Allsopp M (2016) Prevalence and Characteristics of Autism Spectrum Disorder Among Children Aged 8 Years - Autism and Developmental Disabilities Monitoring Network, 11 Sites, United States, 2012. Morb Mortal Wkly report Surveill Summ 65:1–23.

Chuang S-C, Zhao W, Bauchwitz R, Yan Q, Bianchi R, Wong RKS (2005) Prolonged epileptiform discharges induced by altered group I metabotropic glutamate receptor-mediated synaptic responses in hippocampal slices of a fragile X mouse model. J Neurosci

25:8048–8055.

Chung S, Li X, Nelson SB, Street S (2002) Short-Term Depression at Thalamocortical Synapses Contributes to Rapid Adaptation of Cortical Sensory Responses In Vivo. Neuron 34:437–446.

Clancy KB, Schnepel P, Rao AT, Feldman DE (2015) Structure of a Single Whisker Representation in Layer 2 of Mouse Somatosensory Cortex. J Neurosci 35:3946–3958.

Constantinople CM, Bruno RM (2011) Effects and mechanisms of wakefulness on local cortical networks. Neuron 69:1061–1068.

Contractor A, Klyachko VA, Portera-Cailliau C (2015) Altered Neuronal and Circuit Excitability in Fragile X Syndrome. Neuron 87:699–715.

Corder GW, Foreman DI (2009) Nonparametric Statistics for Non-Statisticians: A Step-by-Step Approach. Hoboken: John Wiley & Sons, Inc.

Cossart R (2014) Operational hub cells: A morpho-physiologically diverse class of GABAergic neurons united by a common function. Curr Opin Neurobiol 26:51–56.

Cruz-Martín A, Crespo M, Portera-Cailliau C (2010) Delayed stabilization of dendritic spines in fragile X mice. J Neurosci 30:7793–7803.

D'Antuono M, Merlo D, Avoli M (2003) Involvement of cholinergic and gabaergic systems in the fragile X knockout mice. Neuroscience 119:9–13.

D'Hulst C, Kooy RF (2007) The GABAA receptor: a novel target for treatment of fragile X? Trends Neurosci 30:425–431.

Dana H, Chen T-W, Hu A, Shields BC, Guo C, Looger LL, Kim DS, Svoboda K (2014) Thy1-GCaMP6 Transgenic Mice for Neuronal Population Imaging In Vivo. PLoS One 9:e108697.

Dana H, Mohar B, Sun Y, Narayan S, Gordus A, Jeremy P, Tsegaye G, Holt GT, Hu A, Walpita D, Macklin JJ, Bar CI, Ahrens MB, Schreiter ER, Jayaraman V, Looger LL, Svoboda K, Kim DS (2016) Sensitive red protein calcium indicators for imaging neural activity. Elife.

de Vries B, Severijnen L-A, Jacobs A, Olmer R, Halley D, Oostra B, Willemsen R (2003) FMRP expression studies in blood and hair roots in a fragile X family with methylation mosaics. J Med Genet 40:535–539.

Diamond ME, von Heimendahl M, Knutsen PM, Kleinfeld D, Ahissar E (2008) "Where" and "what" in the whisker sensorimotor system. Nat Rev Neurosci 9:601–612.

Dölen G, Osterweil E, Rao BSS, Smith GB, Auerbach BD, Chattarji S, Bear MF (2007) Correction of fragile X syndrome in mice. Neuron 56:955–962.

Dombeck DA, Khabbaz AN, Collman F, Adelman TL, Tank DW (2007) Imaging large-scale neural activity with cellular resolution in awake, mobile mice. Neuron 56:43–57.

Entezam A, Biacsi R, Orrison B, Saha T, Hoffman GE, Grabczyk E, Nussbaum RL, Usdin K (2007) Regional FMRP deficits and large repeat expansions into the full mutation range in a new Fragile X premutation mouse model. Gene 395:125–134.

Ethridge LE, White SP, Mosconi MW, Wang J, Byerly MJ, Sweeney JA (2016) Reduced habituation of auditory evoked potentials indicate cortical hyper-excitability in Fragile X Syndrome. Transl Psychiatry 6:e787.

Feng G (2016) Dissecting Synaptic and Circuitry Mechanisms of ASD. In: ACNP 55th Annual Meeting.

FRAXA (2014) Novartis Discontinues Development of mavoglurant (AFQ056) for Fragile X Syndrome. www.fraxa.org:1–7.

Frye CG, MacLean JN (2016) Spontaneous Activations Follow a Common Developmental

Course Across Primary Sensory Areas in Mouse Neocortex. J Neurophysiol:jn.00172.2016.

Fu YH, Kuhl DP, Pizzuti A, Pieretti M, Sutcliffe JS, Richards S, Verkerk AJ, Holden JJ, Fenwick RG, Warren ST (1991) Variation of the CGG Repeat at the Fragile X Site Results in Genetic Instability: Resolution of the Sherman Paradox. Cell 67:1047–1058.

Gee KR, Brown KA, Chen WN, Bishop-Stewart J, Gray D, Johnson I (2000) Chemical and physiological characterization of fluo-4 Ca(2+)-indicator dyes. Cell Calcium 27:97–106.

Gibson JR, Bartley AF, Hays SA, Huber KM (2008) Imbalance of Neocortical Excitation and Inhibition and Altered UP States Reflect Network Hyperexcitability in the Mouse Model of Fragile X Syndrome. J Neurophysiol 100:2615–2626.

Goel A, Buonomano D V. (2016) Temporal Interval Learning in Cortical Cultures Is Encoded in Intrinsic Network Dynamics. Neuron 91:320–327.

Goldsmith HH, Van Hulle CA, Arneson CL, Schreiber JE, Gernsbacher MA (2006) A population-based twin study of parentally reported tactile and auditory defensiveness in young children. J Abnorm Child Psychol 34:393–407.

Golshani P, Gonçalves JT, Khoshkhoo S, Mostany R, Smirnakis S, Portera-Cailliau C (2009) Internally mediated developmental desynchronization of neocortical network activity. J Neurosci 29:10890–10899.

Gonçalves JT, Anstey JE, Golshani P, Portera-Cailliau C (2013) Circuit level defects in the developing neocortex of Fragile X mice. Nat Neurosci 16:903–909.

Grant RA, Mitchinson B, Prescott TJ (2012) The development of whisker control in rats in relation to locomotion. Dev Psychobiol 54:151–168.

Green SA, Hernandez L, Bookheimer SY, Dapretto M (2016) Salience Network Connectivity in Autism Is Related to Brain and Behavioral Markers of Sensory Over-Responsivity. J Am

Acad Child Adolesc Psychiatry 55:618–626.e1.

Green SA, Hernandez L, Tottenham N, Krasileva K, Bookheimer SY, Dapretto M (2015) Neurobiology of Sensory Overresponsivity in Youth With Autism Spectrum Disorders. JAMA Psychiatry 72:778.

Green SA, Hernandez LM, Bowman HC, Bookheimer SY, Dapretto M (2017) Sensory over-responsivity and social cognition in ASD: Effects of aversive sensory stimuli and attentional modulation on neural responses to social cues. Dev Cogn Neurosci.

Green SA, Rudie JD, Colich NL, Wood JJ, Shirinyan D, Hernandez L, Tottenham N, Dapretto M, Bookheimer SY (2013) Overreactive brain responses to sensory stimuli in youth with autism spectrum disorders. J Am Acad Child Adolesc Psychiatry 52:1158–1172.

Grienberger C, Chen X, Konnerth A (2014) NMDA Receptor-Dependent Multidendrite Ca(2+) Spikes Required for Hippocampal Burst Firing In Vivo. Neuron 81:1274–1281.

Grienberger C, Konnerth A (2012) Imaging Calcium in Neurons. Neuron 73:862–885.

Grynkiewicz G, Poenie M, Tsien RY (1985) A new generation of Ca2+ indicators with greatly improved fluorescence properties. J Biol Chem 260:3440–3450.

Guo Z V, Hires SA, Li N, O'Connor DH, Komiyama T, Ophir E, Huber D, Bonardi C, Morandell K, Gutnisky D, Peron S, Xu N, Cox J, Svoboda K (2014) Procedures for behavioral experiments in head-fixed mice. PLoS One 9:e88678.

Guy J, Gan J, Selfridge J, Cobb S, Bird A (2007) Reversal of Neurological Defects in a Mouse Model of Rett Syndrome. Science (80-) 315:1143–1147.

Hagerman R, Hoem G, Hagerman P (2010) Fragile X and autism: Intertwined at the molecular level leading to targeted treatments. Mol Autism 1:12.

Hagerman RJ, Amiri K, Cronister A (1991) Fragile X checklist. Am J Med Genet 38:283–287.

Hagerman RJ, Des-Portes V, Gasparini F, Jacquemont S, Gomez-Mancilla B (2014) Translating molecular advances in fragile X syndrome into therapy: a review. J Clin Psychiatry 75:e294-307.

Halsey LG, Curran-everett D, Vowler SL, Drummond GB (2015) The fickle P value generates irreproducible results. 12:179–185.

Harlow EG, Till SM, Russell TA, Wijetunge LS, Kind P, Contractor A (2010) Critical Period Plasticity Is Disrupted in the Barrel Cortex of Fmr1 Knockout Mice. Neuron 65:385–398.

Harris SW, Hessl D, Goodlin-Jones B, Ferranti J, Bacalman S, Barbato I, Tassone F, Hagerman PJ, Herman K, Hagerman RJ (2008) Autism Profiles of Males with Fragile X Syndrome. Am J Ment Retard 113:403–417.

He CX, Portera-Cailliau C (2013) The trouble with spines in fragile X syndrome: Density, maturity and plasticity. Neuroscience 251:120–128.

He Q, Nomura T, Xu J, Contractor a. (2014) The Developmental Switch in GABA Polarity Is Delayed in Fragile X Mice. J Neurosci 34:446–450.

Heiss JE, Katz Y, Ganmor E, Lampl I (2008) Shift in the balance between excitation and inhibition during sensory adaptation of S1 neurons. J Neurosci 28:13320–13330.

Holtmaat A, de Paola V, Wilbrecht L, Trachtenberg JT, Svoboda K, Portera-Cailliau C (2012) Imaging neocortical neurons through a chronic cranial window. Cold Spring Harb Protoc 6:694–701.

Hormigo S, Vega-Flores G, Castro-Alamancos MA (2016) Basal Ganglia Output Controls Active Avoidance Behavior. J Neurosci 36:10274–10284.

Huber KM, Kayser MS, Bear MF (2000) Role for Rapid Dendritic Protein Synthesis in Hippocampal mGluR-Dependent Long-Term Depression. Science (80-) 288:1254–1256.

Iossifov I et al. (2012) De novo gene disruptions in children on the autistic spectrum. Neuron 74:285–299.

Jacquemont S et al. (2011) Epigenetic modification of the FMR1 gene in fragile X syndrome is associated with differential response to the mGluR5 antagonist AFQ056. Sci Transl Med 3:64ra1.

Jacquemont S, Berry-Kravis E, Hagerman R, Von Raison F, Gasparini F, Apostol G, Ufer M, Des Portes V, Gomez-Mancilla B (2014) The challenges of clinical trials in fragile X syndrome. Psychopharmacology (Berl) 231:1237–1250.

Johnston DG, Denizet M, Mostany R, Portera-Cailliau C (2013) Chronic in vivo imaging shows no evidence of dendritic plasticity or functional remapping in the contralesional cortex after stroke. Cereb Cortex 23:751–762.

Juczewski K, von Richthofen H, Bagni C, Celikel T, Fisone G, Krieger P (2016) Somatosensory map expansion and altered processing of tactile inputs in a mouse model of fragile X syndrome. Neurobiol Dis 96:201–215.

Kandel ER, Schwartz JH, Jessell TM (2000) Principles of Neural Science, 4th ed. McGraw-Hill.

Kanner L (1943) Autistic disturbances of affective contact. Nerv Child 2:217–250.

Kerr JND, de Kock CPJ, Greenberg DS, Bruno RM, Sakmann B, Helmchen F (2007) Spatial organization of neuronal population responses in layer 2/3 of rat barrel cortex. J Neurosci 27:13316–13328.

Khatri V, Hartings J a, Simons DJ (2004) Adaptation in thalamic barreloid and cortical barrel neurons to periodic whisker deflections varying in frequency and velocity. J Neurophysiol 92:3244–3254.

Kim J-Y, Ash RT, Ceballos-Diaz C, Levites Y, Golde TE, Smirnakis SM, Jankowsky JL (2013)

Viral transduction of the neonatal brain delivers controllable genetic mosaicism for visualising and manipulating neuronal circuits in vivo. Eur J Neurosci 37:1203–1220.

Kleinfeld D, Ahissar E, Diamond ME (2006) Active sensation: insights from the rodent vibrissa sensorimotor system. Curr Opin Neurobiol 16:435–444.

Kolisnyk B, Guzman MS, Raulic S, Fan J, Magalhães AC, Feng G, Gros R, Prado VF, Prado M a M (2013) ChAT-ChR2-EYFP mice have enhanced motor endurance but show deficits in attention and several additional cognitive domains. J Neurosci 33:10427–10438.

Krzywinski M, Altman N (2013) Points of significance: Power and sample size. Nat Methods 10:1139–1140.

Kuhlman SJ, O'Connor DH, Fox K, Svoboda K (2014) Structural Plasticity within the Barrel Cortex during Initial Phases of Whisker-Dependent Learning. J Neurosci 34:6078–6083.

Lai M-C, Lombardo M V, Baron-Cohen S (2014) Autism. Lancet 383:896–910.

Lee S-H, Dan Y (2012) Neuromodulation of brain states. Neuron 76:209–222.

Liss M, Saulnier C, Fein D, Kinsbourne M (2006) Sensory and attention abnormalities in autistic spectrum disorders. Autism 10:155–172.

Lissek T, Obenhaus HA, Ditzel DAW, Nagai T, Miyawaki A, Sprengel R, Hasan MT (2016) General Anesthetic Conditions Induce Network Synchrony and Disrupt Sensory Processing in the Cortex. Front Cell Neurosci 10:1–14.

Looger LL, Griesbeck O (2011) Genetically encoded neural activity indicators. Curr Opin Neurobiol 22:18–23.

Lovelace JW, Wen TH, Reinhard S, Hsu MS, Sidhu H, Ethell IM, Binder DK, Razak KA (2016) Matrix metalloproteinase-9 deletion rescues auditory evoked potential habituation deficit in a mouse model of Fragile X Syndrome. Neurobiol Dis 89:126–135.

Lu H, Ash RT, He L, Kee SE, Wang W, Yu D, Hao S, Meng X, Ure K, Ito-Ishida A, Tang B, Sun Y, Ji D, Tang J, Arenkiel BR, Smirnakis SM, Zoghbi HY (2016) Loss and Gain of MeCP2 Cause Similar Hippocampal Circuit Dysfunction that Is Rescued by Deep Brain Stimulation in a Rett Syndrome Mouse Model. Neuron 91:739–747.

Lubs HA (1969) A Marker X Chromosome. Am J Hum Genet 21:231–244.

Marco EJ, Hinkley LBN, Hill SS, Nagarajan S (2011) Sensory processing in autism: A review of neuropsychologic findings. Pediatr Res 69:48–54.

Markram K, Markram H (2010) The intense world theory - a unifying theory of the neurobiology of autism. Front Hum Neurosci 4:224.

Martin JP, Bell J (1943) A Pedigree of Mental Defect Showing Sex-Linkage. J Neurol Psychiatry 6:154–157.

McGraw CM, Samaco RC, Zoghbi HY (2011) Adult neural function requires MeCP2. Science (80-) 333:186.

Mégevand P, Troncoso E, Quairiaux C, Muller D, Michel CM, Kiss JZ (2009) Long-term plasticity in mouse sensorimotor circuits after rhythmic whisker stimulation. J Neurosci 29:5326–5335.

Mei Y, Monteiro P, Zhou Y, Kim J-A, Gao X, Fu Z, Feng G (2016) Adult restoration of Shank3 expression rescues selective autistic-like phenotypes. Nature 530:481–484.

Meredith RM, Dawitz J, Kramvis I (2012) Sensitive time-windows for susceptibility in neurodevelopmental disorders. Trends Neurosci 35:335–344.

Michalon A, Sidorov M, Ballard TM, Ozmen L, Spooren W, Wettstein JG, Jaeschke G, Bear MF, Lindemann L (2012) Chronic Pharmacological mGlu5 Inhibition Corrects Fragile X in Adult Mice. Neuron 74:49–56.

Mientjes EJ, Nieuwenhuizen I, Kirkpatrick L, Zu T, Hoogeveen-Westerveld M, Severijnen L, Rifé M, Willemsen R, Nelson DL, Oostra BA (2006) The generation of a conditional Fmr1 knock out mouse model to study Fmrp function in vivo. Neurobiol Dis 21:549–555.

Mineault PJ, Tring E, Trachtenberg JT, Ringach DL (2016) Enhanced Spatial Resolution During Locomotion and Heightened Attention in Mouse Primary Visual Cortex. J Neurosci 36:6382–6392.

Miyawaki a, Llopis J, Heim R, McCaffery JM, Adams J a, Ikura M, Tsien RY (1997) Fluorescent indicators for Ca2+ based on green fluorescent proteins and calmodulin. Nature 388:882–887.

Mostany R, Portera-Cailliau C (2008) A craniotomy surgery procedure for chronic brain imaging. J Vis Exp 5:2–3.

Mullard A (2015) Fragile X disappointments upset autism ambitions. Nat Rev Drug Discov 14:151–153.

Nagai T, Yamada S, Tominaga T, Ichikawa M, Miyawaki A (2004) Expanded dynamic range of fluorescent indicators for Ca(2+) by circularly permuted yellow fluorescent proteins. Proc Natl Acad Sci U S A 101:10554–10559.

Nakai J, Ohkura M, Imoto K (2001) A high signal-to-noise Ca(2+) probe composed of a single green fluorescent protein. Nat Biotechnol 19:137–141.

Niell CM, Stryker MP (2010) Modulation of Visual Responses by Behavioral State in Mouse Visual Cortex. Neuron 65:472–479.

O'Connor DH, Peron SP, Huber D, Svoboda K (2010) Suppl. Info - Neural activity in barrel cortex underlying vibrissa-based object localization in mice. Neuron 67:1–34.

O'Donnell C, Gonçalves JT, Whiteley N, Portera-Cailliau C, Sejnowski TJ (2017) The

Population Tracking Model: A Simple, Scalable Statistical Model for Neural Population Data. Neural Comput 29:50–93.

Ohzawa I, Sclar G, Freeman RD (1982) Contrast gain control in the cat visual cortex. Nature 298:266–268.

Ollerenshaw DR, Zheng HJ V, Millard DC, Wang Q, Stanley GB (2014) The adaptive trade-off between detection and discrimination in cortical representations and behavior. Neuron 81:1152–1164.

Olmos-Serrano JL, Paluszkiewicz SM, Martin BS, Kaufmann WE, Corbin JG, Huntsman MM (2010) Defective GABAergic neurotransmission and pharmacological rescue of neuronal hyperexcitability in the amygdala in a mouse model of fragile X syndrome. J Neurosci 30:9929–9938.

Orefice LL, Zimmerman AL, Chirila AM, Sleboda SJ, Head JP, Ginty DD, Orefice LL, Zimmerman AL, Chirila AM, Sleboda SJ, Head JP, Ginty DD (2016) Peripheral Mechanosensory Neuron Dysfunction Underlies Tactile and Behavioral Deficits in Mouse Models of ASDs. Cell 166:299–313.

Padmashri R, Reiner BC, Suresh a., Spartz E, Dunaevsky a. (2013) Altered Structural and Functional Synaptic Plasticity with Motor Skill Learning in a Mouse Model of Fragile X Syndrome. J Neurosci 33:19715–19723.

Pan F, Aldridge GM, Greenough WT, Gan W-B (2010) Dendritic spine instability and insensitivity to modulation by sensory experience in a mouse model of fragile X syndrome. Proc Natl Acad Sci U S A 107:17768–17773.

Parikshak NN, Luo R, Zhang A, Won H, Lowe JK, Chandran V, Horvath S, Geschwind DH (2013) Integrative functional genomic analyses implicate specific molecular pathways and

circuits in autism. Cell 155:1008–1021.

Parikshak NN, Swarup V, Belgard TG, Irimia M, Ramaswami G, Gandal MJ, Hartl C, Leppa V, Ubieta LT, Huang J, Lowe JK, Blencowe BJ, Horvath S, Geschwind DH (2016) Genome-wide changes in lncRNA, splicing, and regional gene expression patterns in autism. Nature 540:423–427.

Peça J, Feliciano C, Ting JT, Wang W, Wells MF, Venkatraman TN, Lascola CD, Fu Z, Feng G (2011) Shank3 mutant mice display autistic-like behaviours and striatal dysfunction. Nature 472:437–442.

Peron SP, Freeman J, Iyer V, Guo C, Svoboda K (2015) A Cellular Resolution Map of Barrel Cortex Activity during Tactile Behavior. Neuron:1–17.

Petersen CCH (2007) The functional organization of the barrel cortex. Neuron 56:339–355.

Pfeiffer BE, Huber KM (2009) The State of Synapses in Fragile X Syndrome. Neuroscientist 15:549–567.

Picciotto MR, Higley MJ, Mineur YS (2012) Acetylcholine as a neuromodulator: cholinergic signaling shapes nervous system function and behavior. Neuron 76:116–129.

Pieretti M, Zhang F, Fu Y-H, Warren ST, Oostra BA, Caskey CT, Nelson DL (1991) Absence of Expression of the FMR-1 Gene in Fragile X Syndrome. Cell 66:817–822.

Pologruto TA, Sabatini BL, Svoboda K (2003) ScanImage : Flexible software for operating laser scanning microscopes. Biomed Eng Online 2:1–9.

Ramirez A, Pnevmatikakis E a, Merel J, Paninski L, Miller KD, Bruno RM (2014) Spatiotemporal receptive fields of barrel cortex revealed by reverse correlation of synaptic input. Nat Neurosci 17:866–875.

Reddy KS (2005) Cytogenetic abnormalities and fragile-x syndrome in Autism Spectrum

Disorder. BMC Med Genet 6:3.

Reimer J, Froudarakis E, Cadwell CR, Yatsenko D, Denfield GH, Tolias AS (2014) Pupil Fluctuations Track Fast Switching of Cortical States during Quiet Wakefulness. Neuron 84:355–362.

Richards BW, Sylvester PE, Brooker C (1981) Fragile X-Linked Mental Retardation: the Martin-Bell Syndrome. J ment Defic Res 25:253–265.

Richards C, Jones C, Groves L, Moss J, Oliver C (2015) Prevalence of autism spectrum disorder phenomenology in genetic disorders: A systematic review and meta-analysis. The Lancet Psychiatry 2:909–916.

Ringach DL, Mineault PJ, Tring E, Olivas ND, Garcia-Junco-Clemente P, Trachtenberg JT (2016) Spatial clustering of tuning in mouse primary visual cortex. Nat Commun 7:12270.

Rochefort NL, Garaschuk O, Milos R-I, Narushima M, Marandi N, Pichler B, Kovalchuk Y, Konnerth A (2009) Sparsification of neuronal activity in the visual cortex at eye-opening. Proc Natl Acad Sci U S A 106:15049–15054.

Sachidhanandam S, Sreenivasan V, Kyriakatos A, Kremer Y, Petersen CCH (2013) Membrane potential correlates of sensory perception in mouse barrel cortex. Nat Neurosci 16:1671–1677.

Santarelli L (2014) Roche RG7090 Announcement. 7090.

Santoro MR, Bray SM, Warren ST (2012) Molecular Mechanisms of Fragile X Syndrome: A Twenty-Year Perspective. Annu Rev Pathol Mech Dis 7:219–245.

Sato TR, Gray NW, Mainen ZF, Svoboda K (2007) The functional microarchitecture of the mouse barrel cortex. PLoS Biol 5:e189.

Selby L, Zhang C, Sun Q-Q (2007) Major defects in neocortical GABAergic inhibitory circuits

in mice lacking the fragile X mental retardation protein. Neurosci Lett 412:227–232.

Shimono M, Beggs JM (2015) Functional clusters, hubs, and communities in the cortical microconnectome. Cereb Cortex 25:3743–3757.

Simons DJ (1985) Temporal and spatial integration in the rat SI vibrissa cortex. J Neurophysiol 54:615–635.

Sinclair D, Oranje B, Razak KA, Siegel SJ, Schmid S (2016) Sensory processing in autism spectrum disorders and Fragile X syndrome—From the clinic to animal models. Neurosci Biobehav Rev:1–19.

Spencer CM, Alekseyenko O, Hamilton SM, Thomas AM, Serysheva E, Yuva-Paylor L a, Paylor R (2011) Modifying behavioral phenotypes in Fmr1KO mice: genetic background differences reveal autistic-like responses. Autism Res 4:40–56.

Sullivan LM, Weinberg J, Keaney JF (2016) Common statistical pitfalls in basic science research. J Am Heart Assoc 5:1–9.

Sutherland GR (1977) Fragile Sites on Human Chromosomes: Demonstration of Their Dependence on the Type of Tissue Culture Medium. Science (80-) 197:265–266.

Tassone F (2014) Newborn Screening for Fragile X Syndrome. JAMA Neurol 71:355–359.

Tian L, Hires SA, Mao T, Huber D, Chiappe ME, Chalasani SH, Petreanu L, Akerboom J, McKinney S a, Schreiter ER, Bargmann CI, Jayaraman V, Svoboda K, Looger LL (2009) Imaging neural activity in worms, flies and mice with improved GCaMP calcium indicators. Nat Methods 6:875–881.

Tomchek SD, Dunn W (2007) Sensory Processing in Children With and Without Autism : A Comparative Study Using the Short Sensory Profile. Am J Occup Ther 61:190–200.

Tsien RY, Rink TJ, Poenie M (1985) Measurement of cytosolic free Ca2+ in individual small

cells using fluorescence microscopy with dual excitation wavelengths. Cell Calcium 6:145–157.

Tyzio R, Nardou R, Ferrari D, Tsintsadze T, Shahrokhi A, Eftekhari S, Khalilov I, Tsintsadze V, Brouchoud C, Chazal G, Lemonnier E, Lozovaya N, Burnashev N, Ben-Ari Y (2014) Oxytocin-Mediated GABA Inhibition During Delivery Attenuates Autism Pathogenesis in Rodent Offspring. Science (80-) 343:675–679.

Ulanovsky N, Las L, Farkas D, Nelken I (2004) Multiple Time Scales of Adaptation in Auditory Cortex Neurons. Blood Press 24:10440–10453.

van der Bourg A, Yang J-W, Reyes-Puerta V, Laurenczy B, Wieckhorst M, Stüttgen MC, Luhmann HJ, Helmchen F (2016) Layer-Specific Refinement of Sensory Coding in Developing Mouse Barrel Cortex. Cereb Cortex:1–16.

Van der Molen MJW, Van der Molen MW, Ridderinkhof KR, Hamel BCJ, Curfs LMG, Ramakers GJ a (2012) Auditory change detection in fragile X syndrome males: a brain potential study. Clin Neurophysiol 123:1309–1318.

van Karnebeek CDM, Bowden K, Berry-Kravis E (2016) Treatment of Neurogenetic Developmental Conditions: From 2016 into the Future. Pediatr Neurol 65:1–13.

Veeraragavan S, Bui N, Perkins JR, Yuva-Paylor L a, Carpenter RL, Paylor R (2011a) Modulation of behavioral phenotypes by a muscarinic M1 antagonist in a mouse model of fragile X syndrome. Psychopharmacology (Berl) 217:143–151.

Veeraragavan S, Bui N, Perkins JR, Yuva-Paylor LA, Paylor R (2011b) The modulation of fragile X behaviors by the muscarinic M4 antagonist, tropicamide. Behav Neurosci 125:783–790.

Vincent SB (1912) The Function of the Vibrissae In the Behavior of the White Rat. Behav Mon

1:1–82.

Volk LJ, Pfeiffer BE, Gibson JR, Huber KM (2007) Multiple Gq-coupled receptors converge on a common protein synthesis-dependent long-term depression that is affected in fragile X syndrome mental retardation. J Neurosci 27:11624–11634.

Wassink TH, Piven J, Patil SR (2001) Chromosomal abnormalities in a clinic sample of individuals with autistic disorder. Psychiatr Genet 11:57–63.

Wattendorf DJ, Muenke M (2005) Diagnosis and Management of Fragile X Syndrome. Am Fam Physician 72:111–113.

Wheeler AC, Mussey J, Villagomez A, Bishop E, Raspa M, Edwards A, Bodfish J, Bann C, Bailey DB (2015) DSM-5 Changes and the Prevalence of Parent-Reported Autism Spectrum Symptoms in Fragile X Syndrome. J Autism Dev Disord 45:816–829.

Woolsey T a, van der Loos H (1970) The Structural Organization of Layer IV in the Somatosensory Region (S1) of Mouse Cerebral Cortex. Brain Res 17:205–242.

Workman AD, Charvet CJ, Clancy B, Darlington RB, Finlay BL (2013) Modeling transformations of neurodevelopmental sequences across mammalian species. J Neurosci 33:7368–7383.

Wu H-PP, Ioffe JC, Iverson MM, Boon JM, Dyck RH (2013) Novel, whisker-dependent texture discrimination task for mice. Behav Brain Res 237:238–242.

Yan QJ, Asafo-Adjei PK, Arnold HM, Brown RE, Bauchwitz RP (2004) A phenotypic and molecular characterization of the fmr1-tm1Cgr fragile X mouse. Genes, Brain Behav 3:337–359.

Yan QJ, Rammal M, Tranfaglia M, Bauchwitz RP (2005) Suppression of two major Fragile X Syndrome mouse model phenotypes by the mGluR5 antagonist MPEP. Neuropharmacology

49:1053–1066.

Yuste R, MacLean J, Vogelstein J, Paninski L (2011) Imaging Action Potentials with Calcium Indicators. Cold Spring Harb Protoc 2011:pdb.prot5650-prot5650.

Zariwala H a, Borghuis BG, Hoogland TM, Madisen L, Tian L, De Zeeuw CI, Zeng H, Looger LL, Svoboda K, Chen T-W (2012) A Cre-dependent GCaMP3 reporter mouse for neuronal imaging in vivo. J Neurosci 32:3131–3141.

Zhang Y, Bonnan A, Bony G, Ferezou I, Pietropaolo S, Ginger M, Sans N, Rossier J, Oostra B, LeMasson G, Frick A (2014) Dendritic channelopathies contribute to neocortical and sensory hyperexcitability in Fmr1(-/y) mice. Nat Neurosci 17:1701–1709.

Zhao S, Ting JT, Atallah HE, Qiu L, Tan J, Gloss B, Augustine GJ, Deisseroth K, Luo M, Graybiel AM, Feng G (2011) Cell-type Specific Optogenetic Mice for Dissecting Neural Circuitry Function. Nat Methods 8:745–752.

Zwaigenbaum L et al. (2015) Early Identification and Interventions for Autism Spectrum Disorder: Executive Summary. Pediatrics 136:S1 LP-S9.